Global, Seasonal Surface Variations from Satellite Radiance Measurements

WILLIAM B. ROSSOW

NASA Goddard Space Flight Center, Institute for Space Studies, New York, New York

CHRISTOPHER L. BREST

NASA Goddard Institute for Space Studies, New York, New York

LEONID C. GARDER

Columbia University, Department of Geology, New York, New York

(Manuscript received 24 March 1988, in final form 25 September 1988)

ABSTRACT

Global, daily, visible, and infrared radiance measurements from the NOAA-5 Scanning Radiometer (SR) are analyzed for the months of January, April, July, and October 1977 to infer surface radiative properties. A radiative transfer model that simulates the spectral and angular characteristics of the NOAA-5 SR measurements is used to retrieve monthly mean surface visible reflectances and temperature at 25 km resolution. These surface properties were found sufficiently accurate for simulation of clear sky radiances to determine global, seasonal variations in cloudiness. Further comparisons of these results with other data highlight the analysis difficulties and radiative model shortcomings that must be overcome to monitor regional and seasonal variations of earth's surface. These preliminary results also provide an estimate of the magnitude of these variations.

1. Introduction

A major component of the climate system is the surface environment, where exchanges of energy, momentum, water, and other trace gases influence the dynamics of the atmosphere and ocean and where climate perturbations are manifested in alterations of the biosphere. Understanding the role of the surface in the climate system requires characterization of its properties and diagnosis of these exchange processes over the whole globe with sufficient detail to resolve the important scales of variation. This is an objective of the International Satellite Land Surface Climatology Project (ISLSCP) (WCRP 1985a) and of the Tropical Ocean Global Atmosphere (TOGA) project (WCRP 1985b), both part of the World Climate Research Program (WCRP 1984). Determining the global-scale dynamics of the biosphere also requires a systematic survey of the correlations of atmospheric and oceanic phenomena with variations in ecologies. This is the focus of the International Geosphere-Biosphere Program (NAS/NRC 1983).

Although much information must come from in situ surface observations, obtaining an integrated global perspective of the surface system requires analysis of satellite measurements. Monitoring of surface conditions to detect climate-related changes also requires high sensitivity to small variations. These analyses must remove all the effects of the intervening atmosphere, most especially the clouds, and determine the physical properties of the surface from the various radiances measured by satellites, independent of the conditions of observation. As part of a study of the methods to infer cloud properties and cloud-radiative interactions from satellite measurements (Rossow et al. 1989, henceforth, Ro89), we also derived global surface reflectances and temperatures to characterize the global patterns and magnitudes of their regional and seasonal variations. Comparisons of these satellite-based values with surface observations serve to check the accuracy of the cloud detection scheme. Here we use the comparisons to focus on the difficulties that must be resolved to obtain surface measurements with accuracies sufficient for the study of the surface system from satellites.

Of the many analysis techniques that have been developed to obtain surface properties, most determine only relative indices of surface properties rather than their intrinsic values [e.g., see the review in Holben (1986)]. Accurate removal of small variations caused by changes in the radiometer, viewing geometry, and the atmosphere is also not yet routine. Most analyses have generally been employed for studies of specific

Corresponding author address: Dr. William B. Rossow, NASA Goddard Space Flight Center, Institute for Space Studies, 2880 Broadway, New York, NY 10025

sites or regions for limited time periods; only a few global studies covering longer time periods have been undertaken (see Holben 1986; Pinker 1985; Wetzel et al. 1984; McClain et al. 1985). The major exception is the work on retrieval methods for ocean surface temperatures, which aim towards highly accurate measurements of the physical variable (cf., Barton 1985; Njoku 1985), and which are in routine use producing global datasets (Castagne et al. 1986; McMillin and Crosby 1984).

A major obstacle to global, long term analyses is the lack of effective operational techniques for finding data for clear (or cloud-free) scenes in the large satellite datasets; hence, many investigators have selected cloud-free scenes manually. Many cloud analysis techniques have been proposed and studied (see Rossow et al. 1985; Saunders 1986; Rossow et al. 1989), but most of these have not been developed enough for routine application. Recent research and preparations for the International Satellite Cloud Climatology Project (ISCCP) and the First ISCCP Regional Experiment (FIRE) have brought several of these methods up to operational status (see Rossow et al. 1985). Adaptation of these methods for surface remote sensing has already begun, primarily for measurements of the sea surface temperature (e.g., Saunders 1986; Castagne et al. 1986; McClain et al. 1985).

Satellite observations of the surface, which are blocked by the presence of even partial cloud cover, will be limited in their space/time resolution by the cloud variations that are characteristic of each climate regime. Extreme examples are deserts and tropical rainforests; the former are characterized primarily by clear conditions (although dust may be a problem) and the latter are characterized by nearly total cloud cover in the wet season. High time-resolution observations of rain forests may not be possible during some seasons. This drawback is not shared by microwave observations, a technology that is only beginning to be exploited.

Once clear scene radiances have been isolated, the effect of the surface properties on these radiances must be separated from the remaining atmospheric effects. Moreover, since radiances from natural surfaces can vary strongly with wavelength and viewing geometry (e.g., Duggin 1985), determination of the *intrinsic* variations of surface properties requires elimination of these surface effects in the analysis. Although many radiative transfer models have been employed to remove atmospheric effects (e.g., Pinker 1985; Holben 1986; Koepke and Kriebel 1987; McMillin and Crosby 1984), these models do not always explicitly separate the several contributions from the atmosphere and surface as a function of wavelength and geometry. Use of a model that does explicitly represent all of the atmospheric and surface effects requires correlative information about atmospheric and surface properties to complete the analysis of the satellite observations, but this approach has the advantage that it allows for the diagnosis of the separate phenomena that explain the variations in the observed radiances and provides for the kind of correlation studies that are needed to study the interactions of the surface and biosphere with the atmosphere. The Hydrologic–Atmospheric Pilot Experiment (HAPEX) and the First ISLSCP Field Experiment (FIFE) are field programs with an objective to develop and test such analysis methods.

For the past 9 yr, we have been investigating a specific approach to the determination of cloud-radiative feedbacks that combines the information in several datasets with global satellite radiance data into a single consistent radiative analysis. Our investigation has shown that the best cloud detection results are obtained by first isolating the less variable clear scene radiances from the same satellite data and then identifying the clouds by their alteration of the radiances. These clear scene radiances can then be used to determine surface properties. Our focus has been on measuring cloud properties and their radiative effects, but one aspect of this problem is the study of the surface radiation budget. Thus, we have defined radiative model surface parameters so that they can be used to calculate the effect of the surface on both the satellite measured, narrowband radiances and on total radiative fluxes, separately from and together with the atmospheric and cloud effects.

Validation of the cloud detection results is obtained, in part, by validating the *clear scene radiances,* which are calculated in the radiative transfer models from surface and atmospheric parameters. These surface parameters, which are inferred from the satellite measurements using the same radiative models, may represent the radiances adequately, but they may not represent the surface characteristics well enough for the types of studies discussed above. Our focus was to improve the cloud detection method; hence, we provide validation of these surface properties sufficient to determine the accuracy of the cloud detection, but not necessarily sufficient for the study of the surface itself. This validation was done by comparing the satellite-based surface parameters with other conventional observations of the same or related surface properties. This discussion is summarized in Ro89 and section 2f below, but a more detailed discussion of these surface results is presented in this paper.

Section 2 describes the data and the analysis method employed in this study. More details of the analysis method and validation of the cloud/clear separation of the data are given in Ro89. Section 3 presents the comparisons of the satellite-based parameters and other observations of the same or related quantities. It is important to remember that these results were not intended to *resolve* all of the problems: certain corrections or improvements were not attempted because they were not needed to model the clear scene *radiances.* The

importance of these factors is, however, illustrated by the differences between our results and other measurements of the same parameters.

Section 4 discusses the geographic and seasonal variations of surface reflectance and temperature obtained from this analysis; the magnitude of these variations is compared to the uncertainties of measurement discussed in section 3. Section 5 discusses the problem of cloud detection from the perspective of surface studies and summarizes the factors that must be improved in radiative transfer models to obtain accurate measures of intrinsic surface properties.

2. Data and analysis method

a. Satellite radiances

The satellite radiance data used for this study are from the Scanning Radiometer (SR) on the NOAA-5 operational polar orbiting weather satellite from January, April, July, and October 1977. This instrument measures visible (VIS) and infrared (IR) radiances over the wavelength ranges of 0.52–0.72 and 10.5–12.5 μm with a field-of-view (FOV) resolution at the subsatellite point of 4 and 8 km, respectively. The satellite is in a sun-synchronous orbit allowing one daylight (morning) view of each location on earth, except at high latitudes where orbits overlap. Data volume is reduced operationally by limiting observations to satellite zenith angles $\leq 60°$ and sampling the data to allow one observation per day at a 15–25 km spacing. All digital data are obtained from NOAA NESDIS in "polar stereo mosaic" form (NOAA 1977a; Fortuna and Hambrick 1974). All analyses are performed in the original satellite data projections; remapping is done to collect monthly statistics and for convenient display. No results are reported for a month if the number of available observations for a particular location falls below 5.

Visible radiances are reported as coded intensity values divided by the cosine of the solar zenith angle. The NOAA-2 SR was calibrated in a laboratory (Conlan 1973) and verified using an earth target (Jacobowitz and Gruber 1975); comparison of results over the whole NOAA series suggests similar calibrations within 5%–10% (Gruber 1977). The coded values are converted to calibration-source intensities in SI units with a factor 7.70×10^{-3} (watts m^{-2} sr^{-1}) (ft-lamberts)$^{-1}$. Correcting for the spectrum differences between the calibration source and the sun requires multiplying the data values by 1.0538 (see Ro89). The solar constant (1368 watts m^{-2}) multiplied by the instrument response is 260.02 watts m^{-2} (or 82.77 watts m^{-2} sr^{-1}). This calibration is verified to within 5%–10% by comparison of cloud-free reflectivities for ocean and land to literature values (see Matthews and Rossow 1987).

Infrared radiance measurements are calibrated by an on-board blackbody source with known temperature and reported as brightness temperatures with an empirical correction for water vapor absorption as a function of temperature and satellite zenith angle (Conlan 1973; Gruber 1977). The estimated precision of this calibration for the NOAA-5 SR is 2 K. We remove the empirical correction for atmospheric effects and use the "original" brightness temperature values, so that the corrections for atmospheric effects can be made on the observed radiances using our radiative model.

Estimated radiometer noise levels are about 2% for the VIS data and about 2 K for the IR data.

b. Temperature and humidity data

The atmospheric temperature and relative humidity profiles are taken from the twice-daily, gridded analyses produced by the National Meteorological Center (NMC) of NOAA. These data represent an analysis (by assimilation in a forecast model) of conventional weather station reports at 0000 and 1200 UTC every day to produce a uniform map of profiles on standard pressure levels (1000, 850, 700, 500, 300, 200, 100, 50, 10 mb). The map grid defines regions of 2.5° latitude and longitude (for more details, see McPherson et al. 1979; Rosen and Salstein 1980; and Kistler and Parrish 1982). Because the satellite data represent observations at approximately constant local time of day, while the NMC data are for two particular UTCs over the globe, we use the daily average temperature and relative humidity. Uncertainties in these data are estimated to be 3–4 K for temperatures and about 30% for humidities.

The NMC value of surface temperature, TS, is used to calculate the surface pressure, PS, but the surface temperature value used to calculate IR radiances is obtained from a combination of satellite and conventional data as described below. Surface relative humidity is obtained by interpolation when PS < 1000 mb or extrapolation of atmospheric values when PS > 1000 mb. Extrapolation to the surface over land is performed to maintain a constant water vapor mixing ratio below the 1000 mb level, which is more consistent with drier conditions over land. Over ocean, the relative humidity is extrapolated to the surface.

c. Ozone column abundance

Ozone column abundances used in the satellite radiance analysis are specified by the last year of a seasonal, zonal mean climatology obtained by the SBUV on NIMBUS-4, covering the years 1974 through early 1977. (Hilsenrath et al. 1979; Hilsenrath and Schlesinger 1981). Uncertainties are estimated to be about 20%.

d. Other datasets

Five other datasets are used to classify the surface as a function of location: 1) each point on the globe is specified as land or water using a 0.1° resolution world map (derived from Masaki 1972); 2) topographic

heights above mean sea level are taken from the 1° resolution Scripps topography (derived from Gates and Nelson 1975); 3) vegetation type is specified by data from Matthews (1983, 1985); 4) soil type is specified by data from the Oxford World Atlas (1973); and 5) snow-line latitude–altitude climatology by month is taken from Lamb (1972). The first two datasets have been cross-checked against several other standard atlases and a few small errors corrected. The accuracy of the vegetation and soil type maps is discussed in the given references (see also Matthews and Rossow 1987). All of these datasets are used in a statistical analysis of the satellite radiances to obtain maps of the clear sky VIS and IR radiances, as summarized next.

e. Analysis method

Various cloud detection methods have been proposed and are being studied (see Table 1 in Ro89, Minnis and Harrison 1984a; Rossow et al. 1985; Saunders 1986). The method developed and tested in this study is a bispectral threshold method, where cloudy image pixels (one instrument FOV) are identified by the fact that their VIS *and* IR radiances differ from clear scene values. The clear sky values are obtained from a statistical analysis of the time variations of the radiances at each location, augmented by the other data describing the surface characteristics and surface temperatures. Essentially, the satellite radiance data are analyzed twice: first to obtain measures of clear conditions, and second to identify cloudy locations. The steps in the algorithm are as follows: (All analysis steps are performed in the original data projections.)

1) Examine the month-long VIS and IR radiance records at each location to obtain the VIS values corresponding to the four largest IR values, called VIS(IRMAX), and the IR values corresponding to the four lowest VIS values, called IR(VISMIN). These values are converted to surface reflectances (RS) and temperatures (TS) using the monthly mean atmospheric properties and the radiative models described in Ro89.

2) Test the standard deviation (or any other measure of the dispersion) of the four values of RS and TS; in this case, if $\sigma(RS) \leq 5\%$ or $\sigma(TS) \leq 3$ K, then the average of all four values for the individual radiance is taken to represent the surface property. If the standard deviation is too large, this is assumed to be caused by cloud contamination (cf., Sèze and Rossow 1988). In this case, the RS value corresponding to the lowest IR value or the TS value corresponding to the largest VIS value is discarded. If the standard deviation is still not acceptable, no value of RS or TS is reported.

3) To eliminate remaining cloud contamination, collect histograms of the RS values for locations in each latitude zone (90°–60°S, 60°–30°S, etc.) with the same soil or vegetation type (ocean is one surface type); if the width of a histogram is sufficiently small (reflectances at frequencies half of the peak frequency are within −4% and +7%), then RS values which are outside this range on the high side are discarded if they are not consistent with the presence of snow or sea ice cover. A land location is labeled snow covered if its latitude and altitude allow for snow cover during the particular month, based on climatology (Lamb 1972), and the values are RS > 35% and TS* < 273 K. (In this case, TS* is the average of the *largest IR values used to obtain RS, rather than the reported value of TS.*) An ocean location is labeled as sea ice covered if RS > 20% and TS* < 271 K.

4) Fill holes in the global maps of RS and TS, first, using the average RS and TS values over a 5 × 5 pixel array (~100 × 100 km) centered on a missing pixel, if more than 50% of the values are present, and second, using the average values over a larger area (21 × 21 array, ~500 × 500 km). Only land points are used to fill land holes and ocean points for ocean holes. Two flag values are set for each pixel to indicate whether the values of surface reflectances and temperature were obtained in step 2, discarded in step 2 or 3, or filled by the 5 × 5 or 21 × 21 filler in step 4. The resulting maps of RS and TS are taken to represent the monthly mean values. The RS is assumed not to vary significantly in a month, and TS for the ocean is also assumed to be constant over a month.

5) Since TS for land can vary significantly during a month, we combine the daily *deviations* from the monthly mean in the NMC surface temperature data with the satellite monthly mean values to obtain values of TS that vary daily. The mean satellite value is used to correct for the biases introduced by the time-of-day difference between the NMC and satellite observations and by the difference between the surface observable (near-surface air temperature) and the satellite observable (solid surface brightness temperature).

6) Compare each VIS and IR radiance value to a radiative model of the whole atmospheric column, with the atmospheric properties specified by the NMC data, with the surface properties retrieved from the clear sky radiances (steps 1 through 5), and with clouds of varying properties. Any difference between an individual radiance and the model prediction with *no clouds* is interpreted to be due to the presence of cloudiness. The effect of clouds on the VIS and IR radiances are described by two parameters: optical thickness and cloud top temperature. Cloud cover and the optical properties are assumed to be uniform over a single SR FOV.

7) Cloud top temperature (TC), and altitude (ZC) above mean sea level are retrieved by comparing the measured IR radiance with the local daily NMC temperature and humidity profiles, which are converted into two *brightness* temperature profiles for (cosine of the satellite zenith angle) $\mu = 0.5$ and 1.0 using the radiative model. These profiles are interpolated to the appropriate value of μ.

8) Cloud optical thickness (TAU) is retrieved by comparing the measured VIS radiance to a table produced off-line by the radiative model that relates the VIS radiance to TAU values when all the other quantities are specified from other datasets or earlier analysis steps. These model results are available as a function of the viewing geometry and illumination geometry.

9) For clouds with $TAU/\mu < 4$, steps 7 and 8 are repeated to obtain the proper cloud properties accounting for the transparency of the cloud to IR radiation.

10) To avoid spurious detection of clouds because of the uncertainties in the specification of the atmospheric and surface properties, a detection is not claimed unless the radiances at both wavelengths differ from their clear values by more than the estimated uncertainty in the clear sky radiances. Thus, cloud is present in a particular image pixel only if $TAU > 1.6$ *and* $ZC > 1.5$ km. This is equivalent to an uncertainty in the VIS and IR clear sky radiances of 10% and 10 K, respectively.

The NOAA-5 SR data for January, April, July, and October 1977 were analyzed by this method. Surface visible reflectances and temperatures are obtained after steps 1–5. These first steps, though not the complete analysis, were also applied to February 1977 data to test the snow and sea ice detections.

f. Tests of the method

Various tests of the accuracy of the results are discussed in Ro89. These include validation of the retrieved surface reflectances and temperatures, sensitivity studies of the cloud thresholds employed, sensitivity tests of the radiative model of atmospheric effects, and direct comparisons of the cloud properties obtained to other observations. Other internal consistency checks also provide estimates of the errors. Development of the analysis method is an iterative procedure: after devising an initial method, a similar series of accuracy tests is performed and the results are used to refine the analysis method and improve the test parameter values. Thus, the analysis results and validation comparisons, particularly those comparisons discussed here, provide the justification for the analysis method and particular test parameters described above.

The surface property comparisons suggested surface reflectance and temperature errors of < 10% and < 10 K, respectively. Below are brief summaries of the surface property validations from Ro89; these conclusions are supported by the more detailed examination of the surface data comparisons in this paper. We also use these results to determine what factors limit the accuracy of satellite measurements of surface properties.

1) Land surface reflectances. The errors in the land surface visible reflectances caused by incomplete treatment of atmospheric effects and the angular dependence of the surface are judged to be < 3%, absolute, for darker surfaces and as much as 5% for surfaces with reflectances > 50%. These retrieved values incorporate the average effect of the "climatological" aerosols. Persistent or low contrast cloudiness conditions make tropical observations more difficult; even 30 days of observations may fail to obtain clear conditions. Rapid variations of snow cover lead to larger random reflectance errors, ~10% absolute, and several factors (shadowing, aging, cover variations) can also produce biases of this magnitude.

2) Ocean surface reflectances. A Fresnel reflection model used in the radiative calculations is generally successful in predicting the ocean visible reflectances, except in areas of high turbidity or glint. The reflectance error is estimated to be about 2%, generally, and the results suggest that satellite-based reflectance models that are regionally dependent could accurately include the mean turbidity effects. Glint conditions make the ocean reflectance more sensitive to the variations of surface winds. Reflectance errors in the model are about 5% near glint conditions; empirical models may perform better than theoretical models near the glint (cf. Minnis and Harrison 1984a). Sea ice reflectances are more uncertain, both because poor illumination conditions reduce measurement accuracy and because of the larger spatial and temporal variability of the sea ice surface. Errors are estimated to be similar to those for snow covered land—about 10%.

3) Ocean surface temperatures. Random retrieval errors in the sea surface temperatures are about 1–3 K, caused largely by radiometer noise and uncertainties in water vapor amounts. Other techniques, that use multiple spectral channels, significantly reduce the error associated with water vapor. Biases in our results are caused by several factors that were intentionally not included in our model; most of this bias can be eliminated. Cloud contamination at low latitudes remains a significant problem for certain regions. Sea ice surface temperatures have not been studied before. The errors are expected to be associated with emissivity variations and poor time resolution in the satellite based results, producing errors of about 4 K.

4) Land surface temperatures. Random errors in land surface temperatures are caused primarily by poor time resolution, since the variability of land surface temperatures is relatively high. In addition to regionally varying biases caused by emissivity variations, land temperatures retrieved from satellite measurements are biased to clear sky conditions. Both of these biases are diurnally and seasonally varying. Random errors are estimated to be about 6 K for clear conditions.

Although these tests and validation studies show that our radiative model for atmospheric effects needs some improvement in the treatment of water vapor absorption, the primary limiting factor to accurate corrections

of satellite radiances (at 0.6 and 11 μm) is uncertainty in the specification of the atmospheric state. This is particularly true with regard to aerosol effects. Errors at other wavelengths, where atmospheric effects are larger, may be proportionately larger. Cloud contamination can also be a significant problem in some regions where the cloudiness is unusually persistent or difficult to distinguish from the surface. Even if these atmospheric effects can be removed, there are also important errors in retrieval of surface properties from satellite measurements directly associated with the modeling of the surface interactions with radiation.

3. Comparisons

Clouds are the most important modifier of satellite-measured radiances in the "window" portions of the solar and thermal radiation spectrum and they must be accounted for in observing the properties of earth's surface at these wavelengths. Most current methods of cloud detection, used in cloud and radiation budget studies, depend on the accuracy of specifying the clear sky radiances, which depend primarily on surface properties (Rossow et al. 1985; Ro89). Comparison of the clear sky or surface properties inferred from satellite data with other conventional measurements serves to evaluate the effectiveness of the cloud algorithm. This use of the surface measurements is emphasized in Ro89. To develop automated cloud detection methods for surface studies, however, the emphasis needs to be changed; whereas most cloud algorithms are tuned to detect most, but not all of the clouds, for surface studies they must be tuned to remove *all* clouds even at the expense of losing some clear scene data (cf. Saunders 1986). This change in requirements is due to the fact that the effects of even a small amount of cloudiness can be larger than the changes occurring in surface properties.

As discussed in Ro89, there are two particular types of clouds that are especially difficult to detect at VIS and IR wavelengths: cirrus, and low, broken, boundary layer clouds. Cirrus clouds can be very difficult to discern in the VIS radiances, but are more easily detected in the IR. Low-level clouds, on the other hand, are very difficult to detect in the IR, but (usually) easier to detect in the VIS (but not at night). Highly broken boundary layer clouds can be extremely difficult to detect reliably in either the VIS or IR and yet they can produce important alterations of the radiances (e.g., Kaufman 1987; Saunders and Kriebel 1987). Many surface studies employ datasets that contain only the radiances for wavelengths that measure the desired property; however, to insure complete removal of cloud contamination, multi-spectral observations are best. In particular, the VIS (0.6 μm) and IR (10–12 μm) channel data should be used to maximize sensitivity to clouds in the analysis of other observations (see Matthews and Rossow 1987; Saunders 1986; Saunders and Kriebel 1987; Ro89). Notable instances of cloud contamination will be mentioned in the discussion below; however, we generally assume that cloud effects have been removed from our results (see Ro89) and concentrate on other factors that introduce errors in determining the surface properties.

Validation of the values obtained in this analysis is done by examination of the statistical patterns in the space/time distributions of these quantities and by comparison to other measurements of similar or related quantities. The comparison of patterns is crucial to the determination of some sources of error, especially those associated with the surface itself, as will be shown. An important statistical analysis method used to examine surface property patterns is to sort the geographic distribution of surface properties into different, nearly homogenous surface type classes; the shapes of the resulting frequency distribution histograms can provide a measure of uncertainties, can detect anomalous values, suggest other meaningful statistical tests, or even indicate that the original classification is in error. A powerful extension of this approach is to histogram the point-by-point differences between two global sets of observations; the distribution of differences separates bias and random errors and can indicate specific regional problems. The distribution of differences of coincident, colocated subsets of the data can determine the relationship between two observations even if their spatial and temporal coverage are not identical. Where observation density is high enough, direct regressions can be performed to provide a quantitative assessment of the two patterns.

a. Radiance model sensitivity tests

Although atmospheric effects on the satellite-measured radiances are rather small at 0.6 and 11 μm (these spectral channels were selected to maximize the contrast between clear and cloudy scenes by minimizing the atmospheric effects), they can introduce systematic errors that interfere with detection of small surface changes. Therefore, the accuracy of the retrieved values of surface reflectance and temperature is still dependent on the accuracy of the radiative transfer model used to remove the atmospheric effects. The importance of atmospheric corrections is greater at other wavelengths.

The accuracy of the clear scene, narrowband radiances simulated by the models used for this study depends on the magnitude of three types of uncertainties (see also Duggin 1985; Justus and Paris 1985; Le Marshall and Schreiner 1985; Holben 1986; Brest and Goward 1987; Koepke and Kriebel 1987): 1) model shortcuts or approximations to decrease computational load, 2) uncertainties in measurements of atmospheric properties used in the model, and 3) neglected effects of the atmosphere or surface on radiances. Many sen-

sitivity tests have been performed to determine the magnitude of errors associated with these factors (see Ro89 and Tables 1 and 2 herein).

The first type of uncertainty refers to any procedures used to speed the computation that may degrade the accuracy of the model calculations, assuming that the model has perfect input data and accounts correctly for all physical effects. For clear scenes this type of error is estimated to be less than 1% by comparison to more detailed model calculations. The two largest problems discovered were a code error that eliminated the correction for ozone absorption in all the surface reflectance retrievals and the neglect of weak line absorption by water vapor in the thermal infrared. The first problem produces a systematic underestimate of surface reflectances in these particular results ranging from 1%–2% for dark surfaces at middle and low latitudes to 5%–10% for snow and ice surfaces at very high latitudes (Matthews and Rossow 1987). The second problem introduces a 1–2 K bias in retrieved surface temperatures at low latitudes (Grassl 1974; Cutten 1985). Both problems can be corrected. Note that errors of this type in radiative transfer models used for satellite data analysis may be larger than the theoretical limit obtained by using the most accurate radiative transfer theory; this possibility is not commonly discussed (but see, e.g., Luther 1984; Justus and Paris 1985).

The second type of error refers to uncertainties produced directly by measurement errors in the input data (McMillin and Crosby 1984; Barton 1985; Holben 1986; Buriez et al. 1986; Koepke and Kriebel 1987; Minnett et al. 1987). The magnitudes of the radiance errors associated with the uncertainties of ozone and water vapor abundances and of atmospheric temperatures are also summarized in Tables 1 and 2.

TABLE 1. Summary of visible band radiance model sensitivity tests, showing the uncertainty in calculated surface reflectances.

Quantity/feature tested	Test	Estimated uncertainty (%)
Monochromatic approximation	Compare to explicit bandpass simulation	1
Order of polynomial expression	Increase order	1
Interpolation interval	Halve intervals	<2
Radiance noise values	Vary input radiance	2
Surface pressure	Vary ± 50 mb	<1
Ozone abundance	Vary ± 20%*	2
Tropospheric aerosol variation	Add aerosol†	<3
Surface angular dependence	Vary reflectance ± 5%‡	<5
Estimated total		2–5

* Ozone uncertainty estimates from Hilsenrath et al. (1979); variability estimates from Bowman and Krueger (1985).
† Aerosol properties and distribution from Toon and Pollack (1976).
‡ Angular variation estimates from Kimes (1983); depends on surface type.

TABLE 2. Summary of infrared band radiance model sensitivity tests, showing the uncertainty in calculated surface temperatures.

Quantity/feature tested	Test	Estimated uncertainty
Monochromatic approximation	Compare to explicit bandpass simulation	1
Finite layer thickness	Decrease layer thickness	1
Surface humidity approximation	Use full model	1
Angle interpolation	Use full model	<1
Radiance noise values	Vary input radiance	2
Atmospheric temperature profile	Vary ± 3 K*	1
Water abundance	Vary ± 50%†	<2
Water vapor absorption coefficient	Vary ± 50%‡	<1
Tropospheric aerosols	Add aerosol§	<1
Estimated total		2–3K

* Estimated uncertainty based on Smith et al. (1979).
† Estimated uncertainty from Rosen and Salstein (1980).
‡ Uncertainty estimated from study reported in Ro89.
§ Aerosol properties and distribution from Toon and Pollack (1976).

The last type of uncertainty refers to uncertainties caused by the actual model representations of atmosphere and surface radiative effects, which may not account correctly for all aspects of these phenomena (see Chester et al. 1987; Duggin 1985; Holben 1986; Koepke and Kriebel 1987; McMillin and Crosby 1984). The primary atmospheric source of error for surface studies is contamination of the "clear" radiances by aerosols and residual clouds. Although aerosols generally produce smaller effects than residual clouds, much less is known about their characteristics, distribution, and variations. Essentially, aerosols form a very thin persistent "cloud" that alters the angular and spectral distribution of the radiation from the surface (e.g., Deering and Eck 1987; Walton 1985); no generally reliable method for measuring aerosols from satellites is available. The analysis approach used here obtains a measure of surface properties that includes a "climatological" average aerosol effect; this effect could be removed in a second analysis step if mean aerosol properties can be obtained.

Many simplifications of the interaction of radiation with the surface are commonly employed in the analysis of satellite measurements. Some of these factors were also not included in our radiative analysis, since our objective was only to reconstruct the clear scene radiances for specific wavelengths and a limited range of viewing geometries. These factors can account for some of the disagreement between the satellite measurements and other observations; however, the focus

of this paper is on the elucidation of those simplifications of surface effects that can produce significant errors.

b. *Land surface reflectance*

The angular and spectral distribution of solar radiation reflected from land surfaces is controlled by the detailed characteristics of the surface microstructure, including the vertical distribution and orientation of small flat surfaces and the texture and "color" of these surfaces (see e.g., Duggin 1985; Kimes 1983). A global perspective is better obtained by thinking of the summation of these microcharacteristics into various surface types that have specific angular and spectral distributions representing the large-scale integration of these details (see Brest 1987; Brest and Goward 1987; Koepke and Kriebel 1987; Kimes et al. 1987). In this view the most fundamental divisions of the land surface depend on soil and vegetation cover (Holben 1986), together with topographic influences on the geometry. Additional factors that influence the surface reflectance are the moisture content of the near-surface environment and the presence of snow cover. Both the color of vegetation and the moisture content are seasonally variable; hence, the time scale for variations of surface reflectance is generally weeks to months. The primary exceptions to this slow variation are regional changes caused by rapid variations of snow cover (Brest 1987) and/or shorter term moisture variations in arid regions. Arid regions can also exhibit significant changes in vegetation structure associated with seasonal moisture changes.

The retrieval of surface reflectance must also contend with a number of other effects, including neglected short-term changes in atmospheric effects, especially aerosols and unresolved clouds (Deering and Eck 1987; Kaufman 1987), and cloud shadows (Sèze and Desbois 1986; McGuffie and Henderson-Sellers 1986). We focus on measurement of the surface reflectance at 0.6 μm; however, we use this discussion to illustrate the problems which become more important to the inference of the spectrally integrated surface albedo from satellite measurements. We do not discuss the problems of accounting for spectral variations (see Brest and Goward 1987; Pinker and Ewing 1987).

One validation study involved classification of surface reflectances according to vegetation types, which should be equivalent to sorting into approximately homogeneous surface reflectance classes (sorting by soil type did not produce useful classes as discussed in Matthews and Rossow 1987), and classification according to the retrieval quality flags that indicate in which step of the analysis the values were obtained (see section 2e). These results are examined more thoroughly in another paper (Matthews and Rossow 1987); however, Fig. 1 illustrates several different types of radiance histograms obtained from this study. The histograms for tropical and midlatitude forests illustrate the range of reflectance values exhibited by a relatively homogeneous surface type. Dense forest distributions are expected to be narrow, since variations are introduced at 0.6 μm primarily by variations in vegetation density (e.g., the deciduous forest and grassland types exhibit reflectance distributions that are progressively wider), rather than by variations in vegetation structures (Holben 1986; Matthews and Rossow 1987). The width of these histograms is consistent with the expected variations due to the neglected variations in

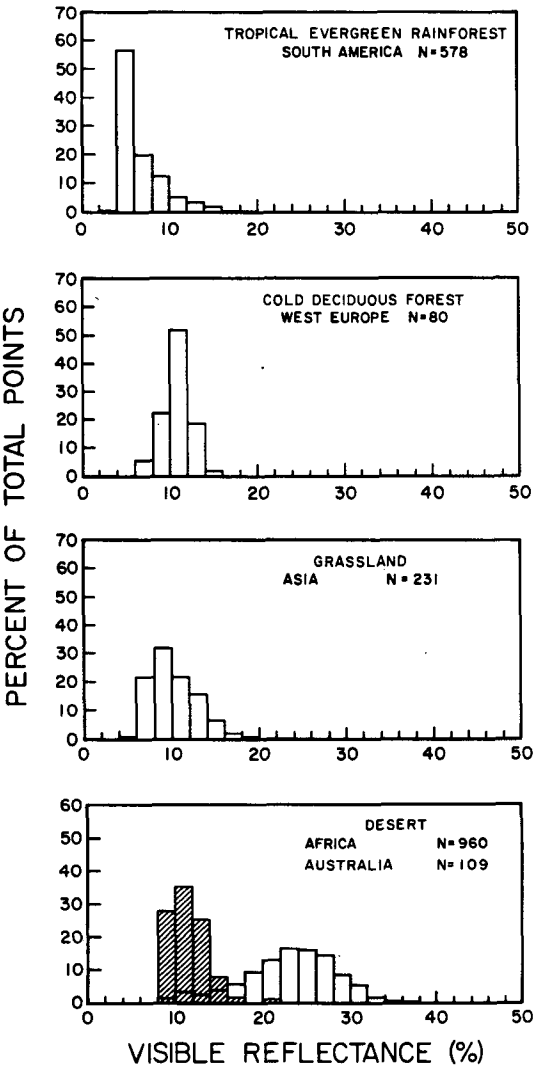

FIG. 1. Distribution of surface visible reflectances deduced from NOAA-5 SR for four vegetation types: (a) tropical rainforest in South America in January, (b) deciduous forest in Western Europe in July, (c) grassland in Asia in July, and (d) desert in Australia in January (shaded distributions) and Africa in July (upper peak). The number of 1° square regions included in each category is shown as the value of N (cf. Matthews and Rossow 1987).

ozone and in the angular dependence of the surface reflectances (cf., Kriebel 1978, 1979; Kimes et al. 1980; Holben and Fraser 1984). In other words, the complexity of the surface reflectance of a forest at this wavelength produces only very small variations in the 0.6 μm radiances measured by a satellite.

The histogram for tropical rainforest should be very narrow, because of the high density of vegetation, but instead a small population of values extends to near 20% reflectance. Comparison of this distribution with the quality flag distribution shows that the higher values are associated with regions with an unusually small frequency of "good" retrievals; i.e., the density of retrievals judged successful according to the tests described in section 2e is much lower than normal. In addition, the comparison of monthly maps (Fig. 2) and histograms (not shown) shows a changing geographic distribution of the anomalously high values that is correlated with anomalously low surface temperatures, leading to the conclusion that these values are produced by contamination due to highly broken cloudiness (cf. Kaufman 1987) or to very persistent (cirrus?) cloudi-

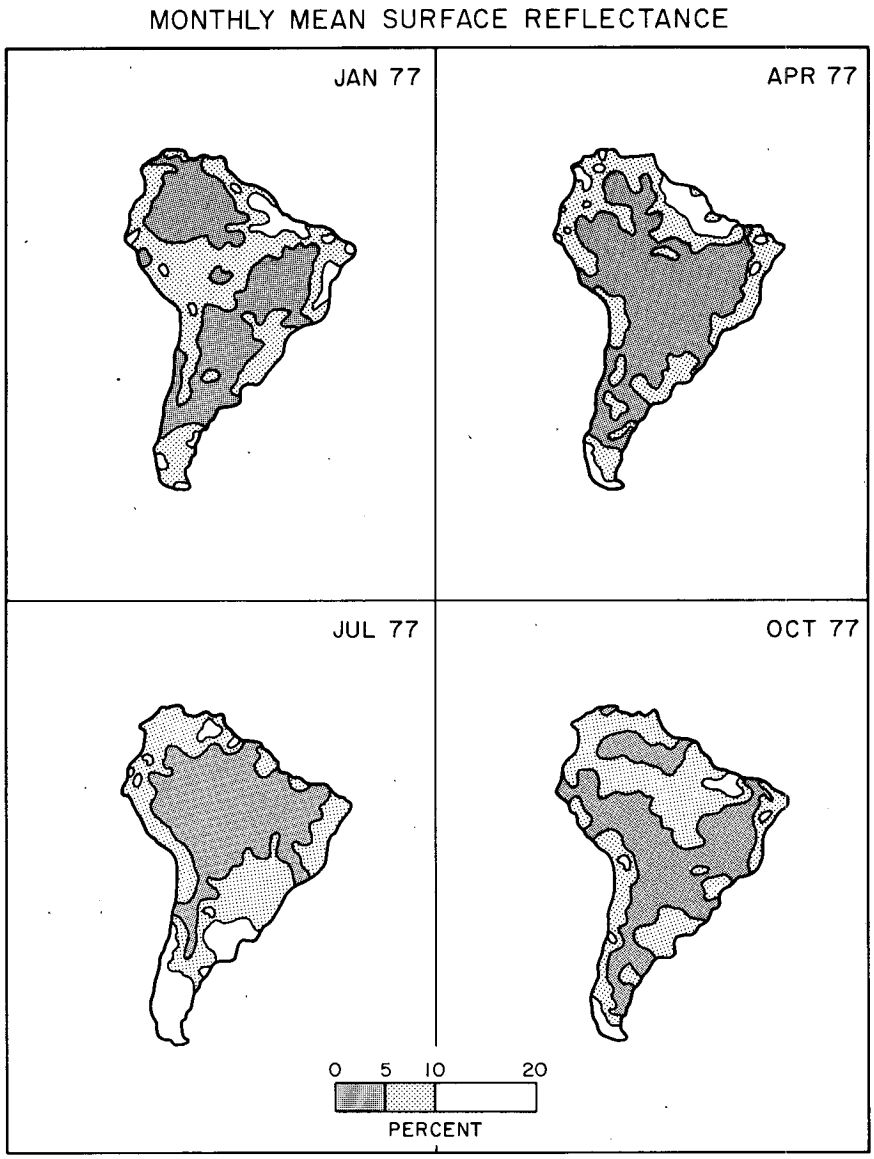

FIG. 2. Monthly mean surface visible reflectance maps of South America from NOAA-5 SR measurements for January, April, July, and October 1977. The dark shading indicates values less than 5%; the light shading indicates values of 5%–10%, and no shading indicates values greater than 10%.

ness (Matthews and Rossow 1987). This is confirmed by the absence of this anomalously bright population in the dry season in July (Fig. 2).

The desert histogram, on the other hand, shows that some surface types are not very homogeneous (cf. Staylor and Suttles 1986); the figure also shows how different two deserts can be. In this and other cases of sparse vegetation cover, however, the distribution shape is found to be nearly constant (within 1%–3%) over the whole year (see Fig. 5 in Ro89), which supports the interpretation that they represent the actual surface properties (Matthews and Rossow 1987). This constancy also means that the variation of the surface reflectance with solar zenith angle is smaller than its variation with location. Nevertheless, brighter bare soil surfaces do exhibit stronger angular dependence; whereas, the spectral dependence is weaker than for vegetation (Brennan and Bandeen 1970; Kimes et al. 1980; Holben and Fraser 1984; Pinker and Ewing 1987).

Specific case studies were also performed to validate the derived spatial patterns apparent in the more heterogeneous areas. Several individual images are selected for each month of data by manual inspection of both VIS and IR images to provide clear views of these locations. Figure 3 shows two samples of the more than 200 scatter plots produced by comparing surface reflectances retrieved from the individual images with the retrieved monthly values for 2.5° square regions. Each point is the daily and monthly reflectances of one or more image pixels, each of which represents an area approximately 15–25 km^2. For dark surfaces (India), the *regional average* monthly and daily reflectances agree well, but the low correlation of the spatial patterns suggests that the variations in these low values are associated with radiometer noise, atmospheric variations (including aerosols), variations of the surface reflectance with viewing geometry, and (possible) contamination by very thin clouds. The angle dependence for this vegetated region is, however, the weakest source of variation for such dark surfaces (Coulson and Reynolds 1971; Holben and Kimes 1986).

For bright surfaces (Sahara), the correlation of the daily and monthly values is excellent. The amount of variability is consistent with the (neglected) anisotropy of desert surfaces (cf., Staylor and Suttles 1986; Holben and Kimes 1986; Coulson et al. 1965). Absolute reflectance values and patterns in western Africa also agree well with other studies of this region (Norton et al. 1979; Courel et al. 1984), if account is taken of the particular wavelength of our observations (see Matthews and Rossow 1987).

Direct comparison of the absolute values of surface reflectance values to other sources of measurement is made difficult by the paucity of such information (see Matthews 1985; Matthews and Rossow 1987; Pinker 1985). Compilations of surface surveys of vegetation types and measurements of the reflectances by type are available (Matthews 1983, 1985), but generally do not provide enough spectral information to verify our results accurately. Other satellite studies either do not remove atmospheric effects (e.g., Briegleb et al. 1986), report only spectrally integrated values, which are often

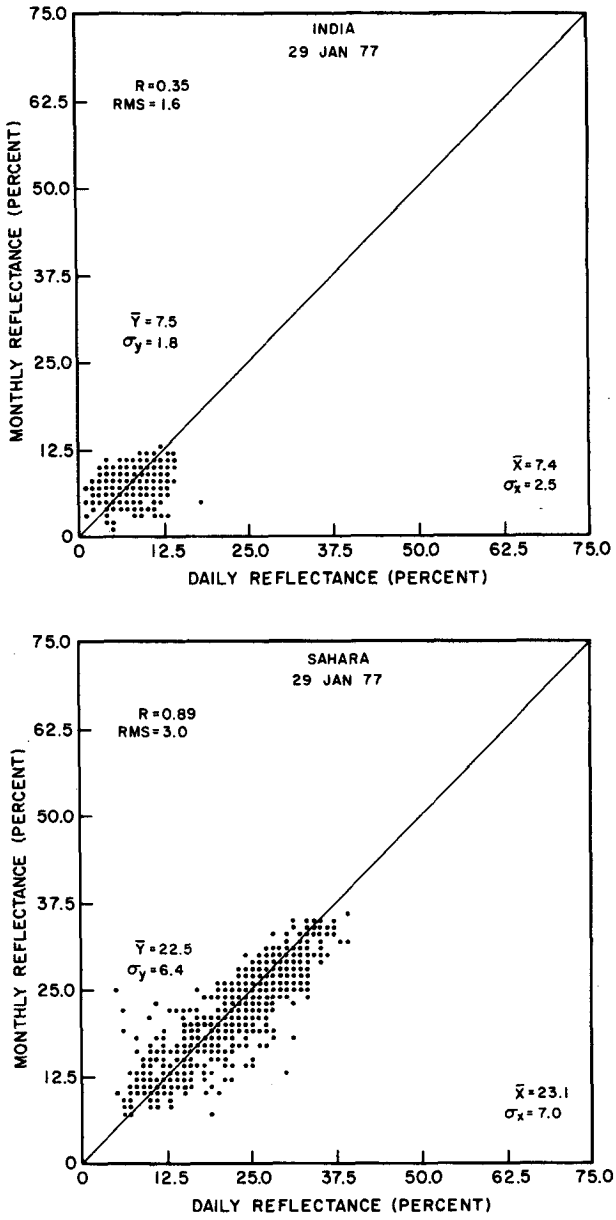

FIG. 3. Comparisons of the surface visible reflectance patterns in the monthly mean to a single NOAA-5 SR image of a 2.5° square region in (a) India and (b) the Sahara on 29 January 1977. The dots represent one or more reflectance values for original image pixels equivalent to areas of 15–25 km^2. The correlation, R, and RMS scatter of the points about a linear best fit are shown; the solid line indicates perfect agreement. The mean and standard deviation of the monthly and daily data are also shown.

derived from narrowband measurements (cf. comparisons in Pinker and Ewing 1987), or do not account for the anisotropy of the reflectance (e.g., Pinty and Szejwach 1985). Comparison with the narrowband values obtained by Kriebel (1978, 1979) and Coulson and Reynolds (1971) shows good agreement for similar vegetation types. Nevertheless, two aspects of the comparison of our values with available information support the validity of these values: average reflectance values for various vegetation types agree with available information and the geographic variations are consistent with known variations of vegetation type (see Matthews and Rossow 1987).

The reflectance of pure snow exhibits significant differences in spectral and angular dependence (Wiscombe and Warren 1980; Warren and Wiscombe 1980; Warren 1982). The spectral dependence is opposite that of soils and vegetation (e.g., Salomonson and Marlatt 1968; Pinker and Ewing 1987), whereas the angular dependence is very weak except for a specular component. However, the rapid variation of snow cover in time, the alteration of snow surfaces by wind and aging processes (Dirmhirn and Eaton 1975), and the interaction of snow with complicated surface structures, especially vegetation (Birnie 1986; Brest 1987; Brest and Goward 1987), makes determination of the surface reflectance in snow covered regions challenging. Currently available data and albedo models of pure snow-covered surfaces still show significant differences (Warren 1982), but the mixture of snow and vegetation produces a complicated and variable spectral/angular-dependence mixture (Birnie 1986; Brest and Goward 1987) that is difficult to predict. Thus, direct comparison of satellite measurements of snow reflectances to ground-based information does not usually provide a very restrictive validation.

Figure 4 shows two examples of many case studies of snow-covered regions, one representing a region that remained covered throughout the month and was far from the melt boundary (central Soviet Union) and one near the melt boundary with varying snow cover during the month (central United States). The reflectance *pattern* on a particular day corresponds very well to the monthly pattern for the Soviet Union,[1] with the magnitude of the remaining variations consistent with the neglected angular dependence (Dirmhirn and Eaton 1975; Warren 1982). This result suggests that the satellite measured values of reflectance (or albedo) for snow-covered surfaces may be the best values available because they can account, empirically, for the geographic and time variations of snow-cover effects. Problems of discriminating between snow and cloudiness need to be resolved, however.

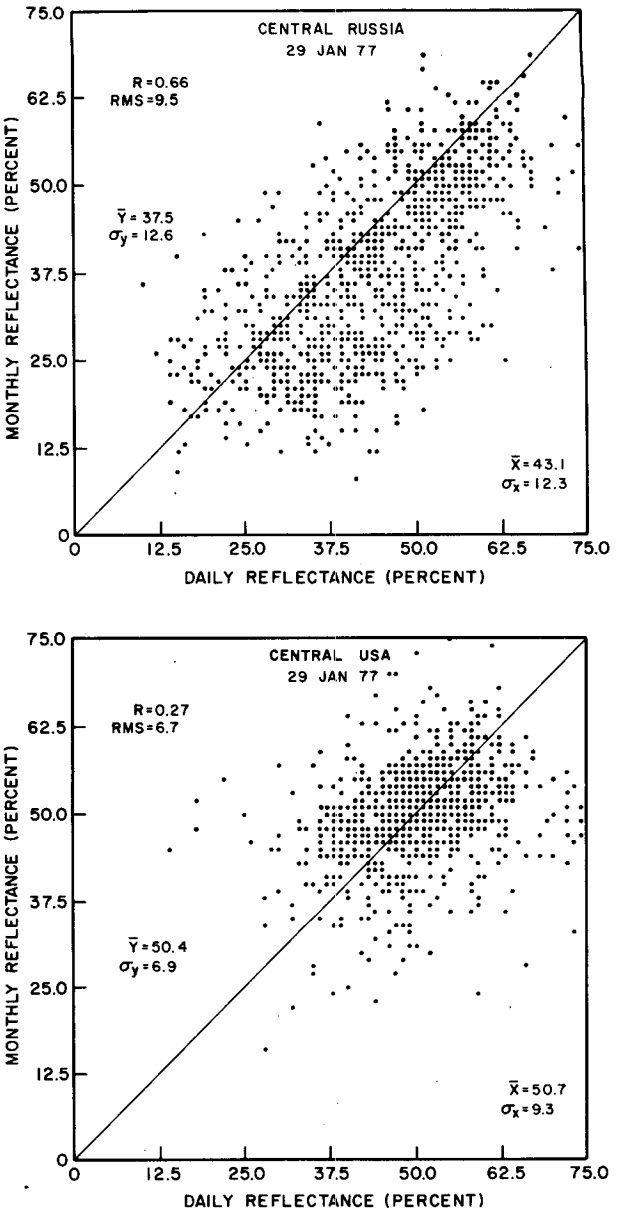

FIG. 4. As in Fig. 3, but for 2.5° regions in (a) central Russia and (b) the central United States.

The case for the central United States shows no correlation between the monthly and daily spatial patterns. However, despite the lack of correspondence in the reflectance *pattern,* the regional mean value is about right. The monthly reflectance pattern differing from a particular daily pattern in an essentially random way may be due to variations in snow-cover amount and aging effects during the month (Dirmhirn and Eaton

[1] The code error that eliminated the ozone absorption correction in the surface reflectance retrieval step causes monthly values at *very high latitudes* to be underestimated by about 5%–10% (see Matthews and Rossow 1987); the small bias in the central Soviet Union results is produced by this effect. At lower latitudes the effect is smaller.

1975), since this region experienced a few snowfall episodes during the month. Other regions in central Canada show more stable conditions like the central Soviet Union case, while regions in the United States that contain the monthly mean snowmelt line show a small negative bias in the monthly mean reflectance. This bias may be explained by the retrieval methodology which selects the *warmest* observations in regions that are not completely snow covered for the whole month. The general amount of variability of snow-covered surface reflectance indicated by these case studies in North America and Asia is consistent with that observed by Robock and Kaiser (1985) and Robinson and Kukla (1985).

General agreement for the absolute values of surface reflectances over Antarctica (Carroll and Fitch 1981; Yamanouchi 1983) was also obtained (subject to correction of the ozone error). Comparisons of other reconstructions of the surface albedo of Greenland and Antarctica (Kukla and Robinson 1980; Robock 1980) suggest that Antarctica is somewhat brighter than Greenland, which is confirmed in our results.

An indirect way to check the validity of our snow reflectances is to compare the snow cover extent inferred from the reflectance patterns with other data. This introduces a problem of interpretation, since we must infer the presence of snow from the reflectances. A review of other methods of inferring the presence of snow from satellite data (Scialdone and Robock 1987) confirms the poor performance of the minimum albedo technique commonly used to detect clear conditions. The effects of snow cover variations and aging (Dirmhirn and Eaton 1975), of terrain mixing of snow and other surfaces (Birnie 1986), and of shadowing by clouds or topographic variations (McGuffie and Henderson-Sellers 1986) all serve to decrease the surface reflectance; hence, the minimum method underestimates the reflectance and the amount of snow present.

Scialdone and Robock (1987) also highlight the difficulties of detecting snow in forested and/or mountainous terrains. Snowfall in a forest hardly alters the reflectance because the trees are not covered by the snow (cf., Brest 1987). Their comparison of various snow data sets leads them to conclude that the NOAA operational snow product (Dewey 1987) is probably the best available indicator of snow cover extent; this is a view shared by Kukla and Robinson (1981). (See Barry 1985, for references to other snow datasets.) However, the quality of the NOAA product is still in doubt for the very rugged Himalayan region (Ropelewski et al. 1984; Dey and Bhanu Kumar 1984).

We compare the snow line location produced by NOAA (1977b) with that obtained from our monthly reflectance values in two ways. Figure 5 shows the United States portion of this comparison: Fig. 5a shows the NOAA snow line superimposed on our monthly mean reflectance map with contours at 20% and 30%;

FIG. 5. Comparison of snow cover inferred from monthly mean surface visible reflectances for North America from NOAA-5 SR data to the NOAA operational snow cover data in January 1977. In (a) the monthly mean surface reflectances are indicated by solid contour lines, 20% (thin solid line) and 30% (thick solid line); shading indicates values < 20%. Hash marks indicate no NOAA-5 data. In (b) the solid contour lines indicate locations where the January mean surface reflectance exceeds the July mean value by > 10% (thick line) and by > 20% (thin line). The NOAA monthly mean snow line is indicated by a dashed line on both maps.

whereas Fig. 5b shows the regions where the January/July reflectance *difference* exceeds 10% and 20%. The comparison between our line and the monthly average

NOAA line is good (within 100 km) in regions where the weekly positions are nearly the same over the month, but poorer (errors of 100–300 km) where the weekly data indicate rapid variations. Figure 2 also shows the inferred snow line position in South America, indicated by the larger reflectance values at high latitudes.

In Fig. 6 we show the seasonal cycle of total surface reflectance obtained from our results; comparisons with other reconstructions of the seasonal cycle of total albedo by Robock (1980), Kukla and Robinson (1980) and Hummel and Reck (1979) show good quantitative correspondence. [There is a systematic bias between our surface reflectances at 0.6 μm and the broadband albedos of these authors (cf., Pinker and Ewing 1987); comparing summer and low latitude values suggests a correspondence between our 10%–15% values and their 20% values.] In particular, the 10% contour of the zonal mean reflectance in the Northern Hemisphere shows a shift from about 65°N in July to about 40°N in January in all results (accounting for the bias). In the Southern Hemisphere, this contour is located at about 65°S in January in all results. Comparisons of monthly surface reflectance maps to the climatology of the snow

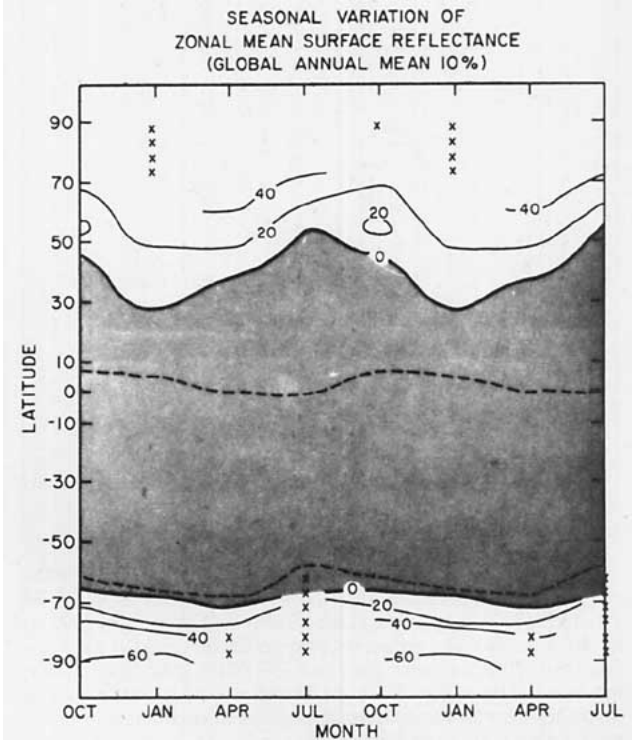

FIG. 6. Seasonal variation of zonal mean surface visible reflectances in percent from NOAA-5 SR data for January, April, July, and October 1977. Solid contours indicate 20% intervals in the zonal mean as deviations with respect to the annual global mean value; the dashed contour is a deviation of 5%. Shading indicates negative deviations and x-marks indicate no measurement is available. The four monthly values are repeated to produce two seasonal cycles.

line position in Robock (1980) also show an excellent correspondence of the large-scale patterns: for example, 1) in January in North America, the snow line is near 40°N with a trend from northeast to southwest; 2) in January in Asia, the snow line is between 42° and 45°N with southern extensions between the Black and Caspian seas into Turkey and into eastern China; and 3) in October in North America, the snow cover is located west of Hudson's Bay and in and north of the coastal mountain ranges in Alaska.

In summary, the uncertainty of the land surface reflectances, due to incomplete treatment of atmospheric and angular effects, is judged to be $\leq$3% at 0.6 μm, if the variability exhibited in the various tests is assumed to be entirely due to analysis problems (see Matthews and Rossow 1987). This uncertainty appears to be random, except for a few tropical regions with cloud contamination. Brighter surfaces, e.g., the Sahara, have somewhat larger errors due to the larger angle dependence. This result should not be taken to mean that the angular dependence of surface reflectances can be ignored in all cases. Rather, this result shows that at 0.6 μm the geographic variations in reflectance, controlled by vegetation density variations, are larger than the errors in correcting for the atmosphere and the surface anisotropy. Using data from a sun synchronous polar orbiter also limits the range of angles encountered (cf. Robock and Kaiser 1988). The same is not true for other wavelengths (cf. Koepke and Kriebel 1987; Kimes et al. 1987) for other satellites, or for monitoring of seasonal variations. Moreover, since the vegetation density variations produce reflectance variations of only about 5%–15%, detection of vegetation changes in observations near this wavelength will require a much more accurate treatment of the satellite data. Sufficiently accurate surface albedos for radiation budget calculations also require proper treatment of the anisotropy (Koepke and Kriebel 1987; Kimes et al. 1987).

Measuring surface properties of certain land areas is made very difficult by unusually persistent cloudiness. The most notable problem areas are the West African coastal zone along the Gulf of Guinea (from Guinea to Congo), Bangladesh and eastern India, southern China and Southeast Asia, the islands in the tropical western Pacific, and the northern and eastern areas of the Amazon Basin.

The rapidly varying parts of the snow-covered land have a larger uncertainty in the reflectances ($\approx$10%). [The error caused by the failure to remove ozone absorption effects is only significant at higher latitudes for brighter surfaces (Matthews and Rossow 1987) and can be corrected.] The error can be decreased somewhat by taking account of the anisotropy of snow-covered surfaces; however, models may have to be developed directly from satellite observations for a very wide variety of surface types (e.g., snow cover on different veg-

etation types). Some decrease in the error may also be possible by increasing the time resolution; however, this requires a more reliable method for distinguishing snow from clouds (e.g., Bunting and d'Entremont 1982). A systematic survey of the effects of snow on surface albedo is possible from satellite data, but such studies have been limited.

The complete geographical distribution of the annual mean land and ocean surface reflectance is shown in Fig. 7 for 1977. The well-known features are apparent: bright North African deserts, generally dark continents which are still brighter than the ocean, and a brightening of land and ocean at higher latitudes by snow and sea ice cover. The level of surface detail that can be examined with a systematic satellite survey is apparent, even at the 1° resolution of Fig. 7; survey of the whole globe at a resolution of 10–30 km seems practical (cf. Tucker et al. 1986). A more detailed study of the five monthly maps of land reflectance is discussed in Matthews and Rossow (1987).

c. *Ocean surface reflectance*

The ocean reflectance as a function of angle is accounted for in the cloud analysis by the model described in Ro89; however, this model includes only the effect of Fresnel reflection from a spectrum of sloping surfaces (also see Takashima and Takayama 1981). Other effects that alter the reflectance of the ocean surface are wind roughening that causes surface bubbles, and suspended particles that significantly increase the reflectance from below the surface (Tanaka and Nakajima 1977).

The statistical retrieval of the surface reflectance can be used to check the validity of our reflectance model by saving the results as a function of geometry. (Minnis and Harrison 1984a, also use a statistical retrieval to develop an empirical model of *planetary* reflectance over ocean.) This comparison shows that the model is correct to within ~2% for geometries away from glint conditions ($\mu \approx \mu_0$, $\phi < 20°$), but that, as glint conditions are approached, the model reflectance does not increase as rapidly as observed. A similar conclusion is reached from a comparison of the model reflectance to other data (e.g., Kondratyev 1969, 1973; Payne 1972). For the geometries encountered by NOAA-5, the discrepancy reached ~5% near the edge of an individual orbit swath (low μ). The gradual brightening of the ocean surface reflectances in Fig. 7 is consistent with the solar zenith angle dependence shown in other measurements (Payne 1972), although some cloud contamination may contribute to the increased reflectances in the southern oceans.

The comparison of the model and retrieved reflectances also uncovered another "discrepancy": several regions of "anomalously" high reflectances were found

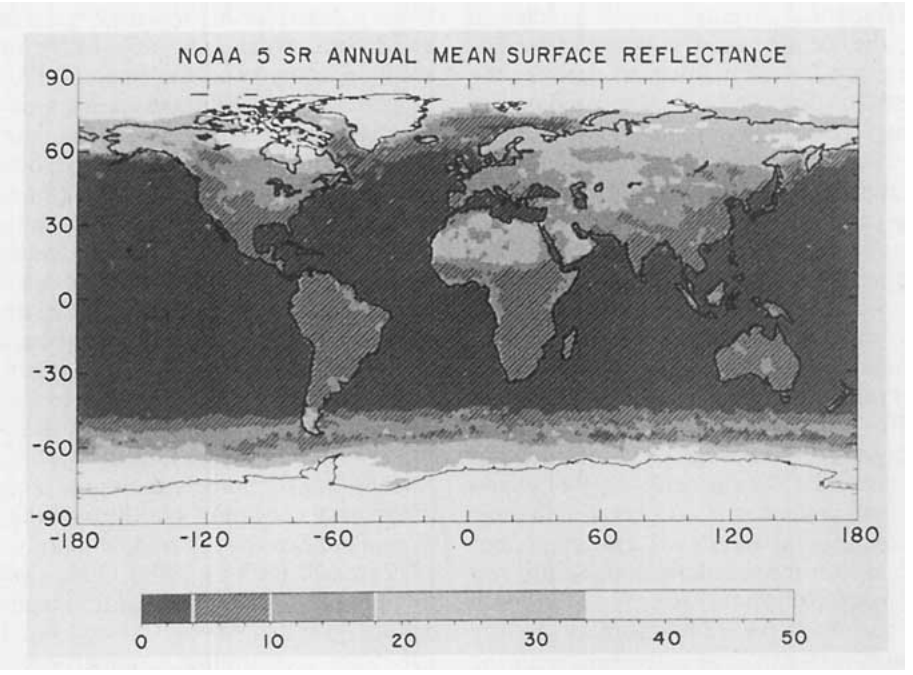

FIG. 7. Geographic distribution of annual mean surface visible (0.6 μm) reflectance in percent from NOAA-5 SR data for 1977. Values are averaged to 1° resolution represent the mean of values for January, April, July, and October, except at latitudes > 65° where no value is contributed from the winter month (see Fig. 6). Hash marks divide the gray scale at the annual global mean surface reflectance. Even though the gray scale has an upper limit of 50%, the white color indicates all values > 34%; most of Greenland and Antarctica have larger reflectances (see Fig. 6).

that appear to correspond to regions of high biological activity and turbidity associated with upwelling motions (FAO 1972). The "anomalous" reflectances were typically twice that expected from the model, i.e., 4%–8% instead of 2%–4%, and consistent with measurements of the highly turbid waters found in such regions (Tanaka and Nakajima 1977). This explanation is strengthened by the absence of only one major region in our reflectance maps, namely, the region off the coast of Peru, consistent with the fact that 1977 was an El Niño year (Miyakoda and Rosati 1982). Measurement and interpretation of this variation of ocean reflectance is the objective of the Coastal Zone Color Scanner (see references in Esaias et al. 1986). These features do not show in Fig. 7 because of averaging over large regions ($\approx 100 \times 100$ km) and all four months.

When sea ice is determined to be present, the ocean model surface reflectance is replaced by the retrieved value of RS. The test for cloud contamination over ocean included a test for sea ice; namely, RS > 20% and TS* < 271 K is required (see section 2e). These criteria are meant to approximate observations representing partial ice cover ($\approx$25%) over the SR FOV, since a brightness temperature of 271 K corresponds to a water surface temperature of about 273 K. The RS criterion is similarly resolution dependent (cf. discussion in Comiso and Zwally 1982).

The surface reflectance of sea ice is sensitive to a number of factors, such as the fractional coverage of open water, the fractional coverage of melt puddles on the ice surface, the ice age, snow cover, and surface roughness. There are few climatological data for the reflectances of sea ice that can be used to validate our values. The *range* of values obtained, 30%–60%, is consistent with available reports of *broadband* albedos for the Arctic (Grenfell and Maykut 1977; Barry 1983; Barry et al. 1984) and the Antarctic (Kuhn and Siogas 1978; Yamanouchi et al. 1986). Grenfell and Perovich (1984) show sea ice albedos in the Beaufort Sea in this same range. Broadband albedos are expected to be lowest in the Arctic in June–August because of melt water on the surface, with typical values about 30%–50%, but the summertime albedos in the Antarctic are expected to be 10%–20% larger because surface melting is less prevalent (Andreas and Ackley 1982; Kuhn and Siogas 1978). Our results show generally higher values in the Antarctic than in the Arctic, consistent with these summaries. These general values are also consistent with the surface albedo reconstructions of Kukla and Robinson (1980) and Robock (1980).

The regional pattern of sea ice reflectances for July 1977 in our results is in excellent agreement with the survey by Scharfen et al. (1987) using the Defense Meteorological Satellite Program (DMSP) imagery, which covers the 0.4–1.1 μm wavelength range. The differences in radiometer spectral responses can account for the small differences in reflectances ($\sim$5% absolute). Scharfen et al. (1987) divide the Arctic basin into five subregions; their monthly mean albedos for July 1977 are 0.52 (central Arctic), 0.42 (Beaufort/Chukchi seas), 0.40 (East Siberian/Luptev seas), 0.27 (Kara/Barents seas), and 0.46 (northwest North Atlantic). Values retrieved from our NOAA-5 SR analysis for the same month and regions are (after correcting for the neglected ozone absorption) 0.5, 0.35, 0.35, 0.3, and 0.4, respectively.

The wide range of sea ice albedo values reported in climatologies and employed in climate models (also see Barry et al. 1984), together with the large spatial variations seen in our results, suggest a need for more careful satellite surveys to monitor the seasonal and geographic variations of the sea ice surface properties.

As with snow, the determination of the location of sea ice can be used as an indirect check on our results. The location of the sea ice edge depends on the treatment of broken ice; i.e., the ice edge must be defined by an ice concentration threshold, above which the area is considered to be ice covered. (This is the same problem encountered in the detection of clouds.) Consequently, intercomparisons of the sea ice edge location in data which sense different properties of the scene and employ different definitions of the threshold ice concentration cannot provide detailed verification (also see Carsey 1982, for discussion of other factors in the analysis of microwave data). For example, Walsh and Johnson (1979) found that disagreements among different datasets for Arctic sea ice positions were as much as 500 km, which is as large as the interannual variability. Sturman and Anderson (1985) find differences in estimates of Antarctic sea ice area from the same data sources of as much as 25%. Use of a single IR channel criterion does not produce detailed agreement with microwave determinations (for example, Zwally et al. 1983); however, our two channel requirement produces a qualitatively similar relationship to that of Zwally et al. (1983) between the sea ice line and the 271 K isotherm in the Weddell Sea area.

Figure 8 shows a comparison of our results with several other datasets for selected, *more highly variable regions* (see Barry 1986 for references to other sea ice data), using two different criteria: RS > 20% and TS* < 271 K (dashed line), and RS > 25% and TS* < 269 K (solid line). Figure 8a shows the mean and the maximum and minimum positions of the ice edge in the Greenland Sea for the middle of July, averaged from 1972 to 1982 (NOAA 1984). Other climatologies based on similar or microwave data and representing the end of July (Wadhams 1981; Carsey 1982; Parkinson et al. 1987) are very similar. Comparisons of sea ice edge positions in the Kara/Barents seas in 1977 (Barry et al. 1984) and the Beaufort/Chukchi seas in 1976 (Parkinson et al. 1987) show agreement to within 100 km (not shown). Given the variations introduced by different definitions of the ice edge location and the time

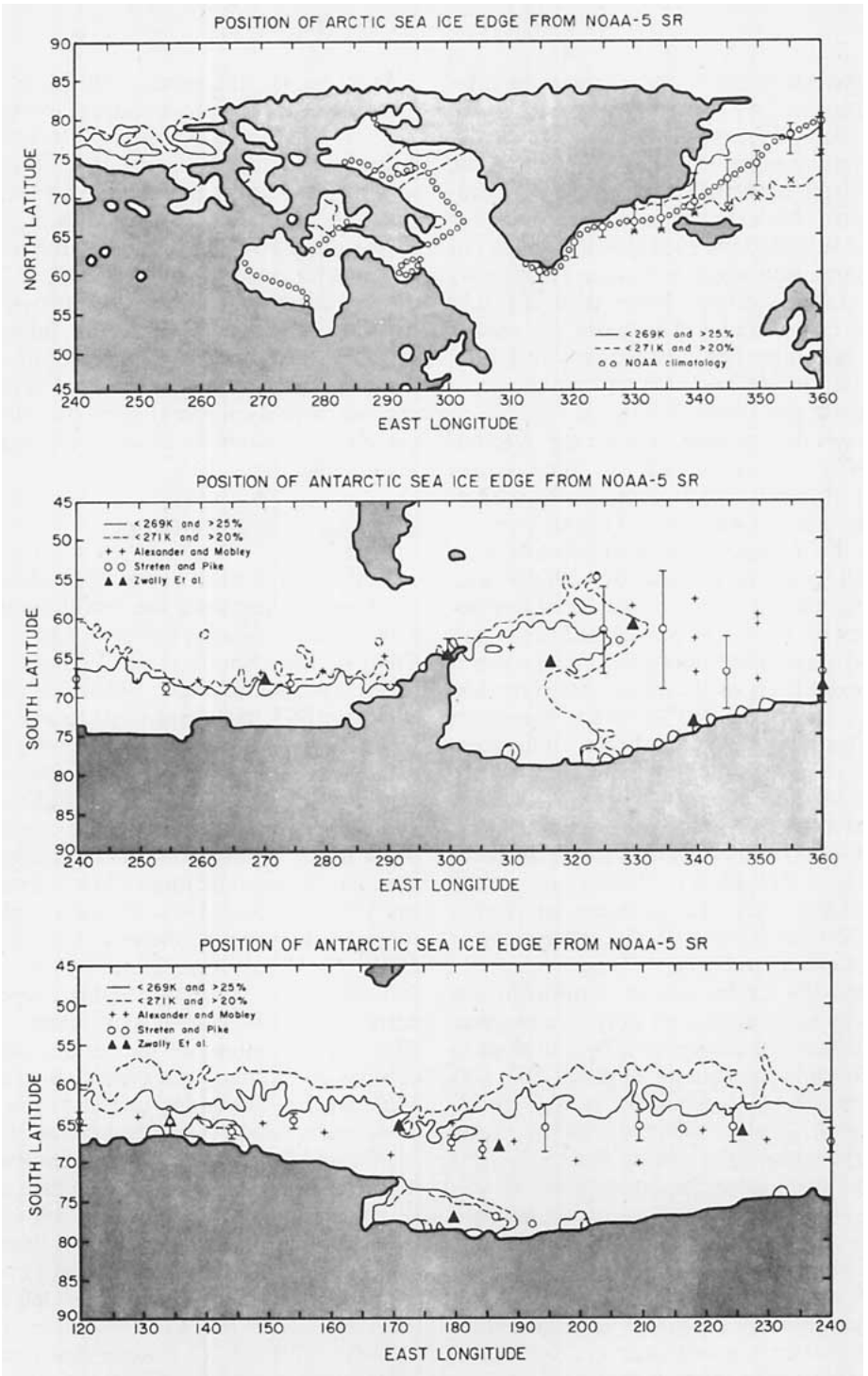

FIG. 8. Comparisons of sea ice boundaries inferred from NOAA-5 SR visible and infrared measurements to sea ice climatologies. Land areas are indicated by shading. The dashed contour indicates sea ice by surface reflectances > 20% *and* surface temperatures < 271 K; the solid contour is for surface reflectances > 25% *and* surface temperatures < 269 K. (a) In the vicinity of Greenland in the middle of July, the open circles show the mean sea ice edge from the NOAA (1984) climatology from 1972 to 1982. The error bars indicate the range of July sea ice edge positions over this 10 yr period; the x-marks indicate extreme ice edge for the beginning of July. (b) In the vicinity of the Weddell Sea in January, the plus mark are the climatology of Alexander and Mobley (1976) and the open circles are that of Streten and Pike (1980). The error bars indicate the variability of January sea ice edges over the years in the Streten and Pike climatology. The solid triangles are the sea ice edge from January 1976 from microwave measurements (Zwally et al. 1983). (c) In the vicinity of the Ross Sea in January, the symbols have the same meaning as in panel (b).

periods which the results cover, the comparison is favorable. Since our method "accepts" any time-stable value from any part of the month, our results cannot account for variations in ice edge that occur within the month. To illustrate how this factor affects the comparison, we indicate the extreme ice edge reported for the beginning of July (NOAA 1984) by the x-marks in Fig. 8a. This comparison suggests that our results may represent early July conditions better than late July conditions. The correspondence between our results and the NOAA operational product for early July 1977 (NOAA 1977b) is, in fact, much better than the comparison to climatologies shown in Fig. 8a.

Figure 8b shows the ice edge data for the Weddell Sea in January 1977 compared with two climatologies (Alexander and Mobley 1976; Streten and Pike 1980) and to the 1976 data of Zwally et al. (1983). The correspondence to the microwave results of Zwally et al. (1983) is especially good and is consistent with the other data, considering the large interannual variability occurring in this region [shown as bars in the Streten and Pike (1980) data]. Agreement among these data is much better along the portions of the coast that show less variability (e.g., longitude 240°–280°E). Figure 8c shows a polyna (open water within the ice) in the Ross Sea that appears to be a remnant of a much larger, but decaying region of open water observed by the NIMBUS-5 microwave in previous years (Zwally et al. 1983). Although no specific data are available for comparison in 1977, confirmation of details such as the polyna suggest that our ice edge positions are correct to within 100–300 km (subject to the uncertainty of the threshold ice concentration).

At first, the results for the winter months do not appear to be as good; comparisons of sea ice position inferred from surface reflectances > 20% (not shown) suggest a bias towards the equator of about 300–500 km. This could be related to persistent ice edge cloudiness (cf. Barry et al. 1984), combined with the effects of low illumination (the solar zenith angle is > 70°) and (relatively) large radiometer noise. These conditions, together with rapid variations of the surface properties, themselves, nearly eliminate successful surface retrievals near the ice edges. Consequently, the surface properties are "filled in" by step 4 of the procedure, producing values of the surface reflectance that are intermediate between open water and ice cover. However, the reflectances of open ocean are already >20% at the solar zenith angles near the ice edge (Payne 1972; Kondratayev 1969); thus, the reflectance contrast between open water and sea ice is, in fact, small. The difficult observing conditions, together with the solar zenith angle dependence of water reflectance makes judging the location of the ice edge by the visible reflectance values very difficult. The correspondence between the monthly mean 271 K isotherms and the ice line position is much better (Fig. 11), suggesting that the reflectance results may not be too bad.

In summary, the model used for ocean surface reflectance is accurate to within 2% except near glint geometry, where the model is 5% below the observed reflectivity. Limited regions of the ocean also exhibit reflectances 2%–6% higher than typical values due to suspended particulates. Detection of this small effect in the data, however, confirms the overall accuracy estimate for most surface reflectances. The uncertainties in the reflectances for sea ice covered regions are harder to estimate; however, the difficulties with the proper identification of clear scenes in these regions, the low illumination, and the amount of variation that can occur in a month suggest that the uncertainties could be 10%, with the larger errors occurring near the sea ice edges.

d. Ocean surface temperature

Remote sensing of sea surface temperature (SST) has been studied since the first satellites began measurements of infrared radiation (e.g., LaViolette and Chabot 1969; Smith et al. 1970; Vukovitch 1971; Shenk and Salomonson 1972b). Techniques for retrieval of SST have continued to improve, such that errors today are estimated to be <1 K for monthly mean values averaged over regions $\approx$ 200–500 km across (Njoku 1985; McClain et al. 1985; Ho et al. 1986). The remaining uncertainty is produced by lack of accurate measurements of atmospheric temperature structure (Maul and Sidran 1973; Bernstein 1982; Barton 1983; Ho et al. 1986; Minnett et al. 1987); atmospheric water vapor abundance (Maul et al. 1978; Maul 1981; McMillin and Crosby 1984; Barton 1985; Schluessel et al. 1987); atmospheric aerosol variations, particularly those caused by volcanos (Walton 1985); emissivity variations of the surface with viewing geometry and surface roughness (Buettner and Kern 1965; Singh 1984); and by uncertainty in the calibration of the radiometers (e.g., Castagne et al. 1986). A limitation on testing improvements in satellite measurements is the accuracy of the ship data usually used to verify the satellite results (Barnett 1984; McClain et al. 1985; Barton 1985; Wright 1986). In particular, conventional ship and buoy data do not measure the skin temperature sensed by the satellite radiometer (Schluessel et al. 1987).

These estimates all assume that there is no cloud contamination of the satellite measurements; however, there are some regions where complete elimination of clouds from the data is very difficult (Maul and Sidran 1973; Bernstein 1982; McClain et al. 1985; Saunders 1986). The statistical tests of the technique used here also reveal small regions in the tropics and subtropics that exhibit some cloud contamination; otherwise, the SST values obtained appear accurate to within 2 K for the smaller regions that we use ($\approx$100 km across).

Figure 9 shows histograms of point-by-point differences between our monthly satellite values and the col-

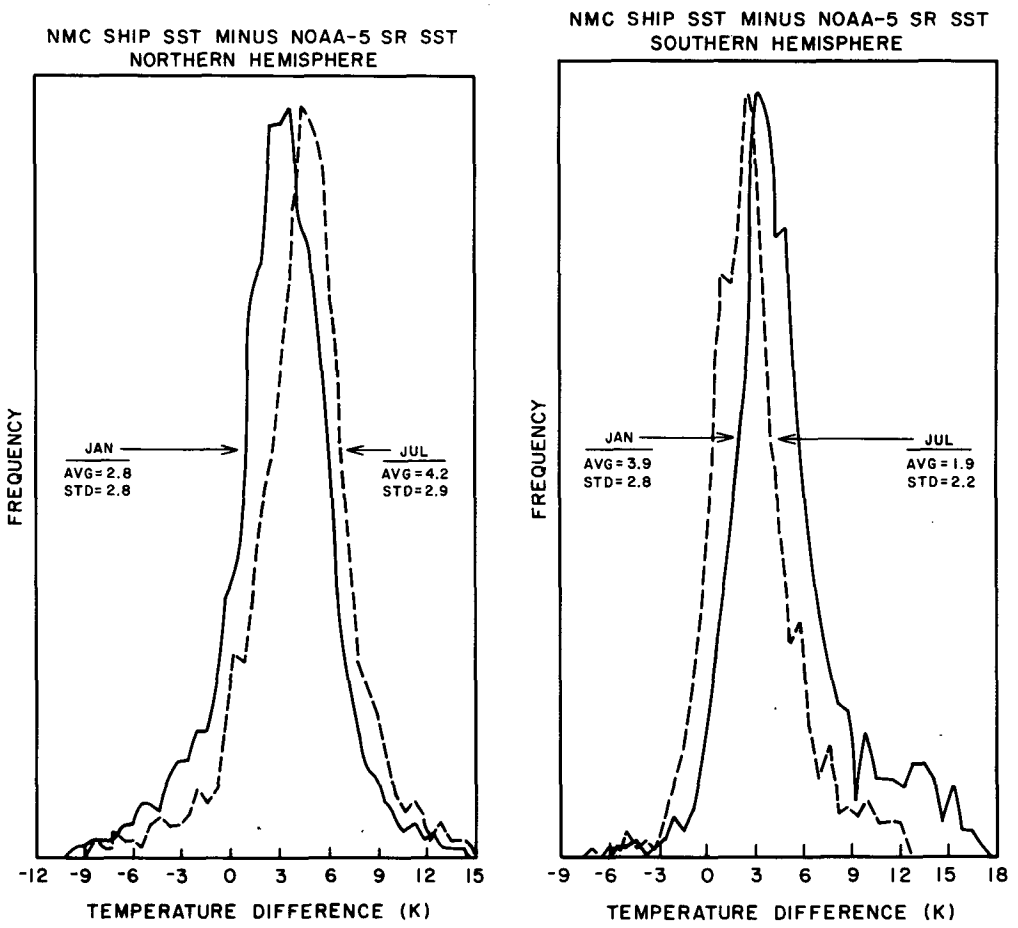

FIG. 9. Distribution of the differences between the monthly mean sea surface temperatures from the NMC ship data and the NOAA-5 SR analysis for January (solid) and July (dashed) 1977 in (a) the Northern Hemisphere and (b) the Southern Hemisphere. The average difference and the standard deviation of the differences are also shown.

located monthly average ship observations. The narrow distributions are consistent with the estimated effects of the atmospheric, surface emissivity, and radiometer uncertainties discussed above. The bias of 2–4 K can be accounted for by four effects: surface emissivity, water vapor absorption, "skin" vs "surface" effects, and calibration. The first two effects can be removed in an improved radiative model, whereas the second two effects are related to data quality. Our retrieved values correspond to the temperatures for a blackbody; correcting the values using the actual emissivity of water (reported as 0.99 by Buettner and Kern 1965, and as 0.98 by Singh 1984) decreases the bias by about 1 K. The actual emissivity depends on the surface roughness (Singh 1984) and the presence of any contaminants on the surface (Buettner and Kern 1965). The emissivity for rough surfaces also depends on the satellite zenith angle, varying between 0.99 and 0.95 as the zenith angle varies from 0° to 60° (Buettner and Kern 1965). This effect was neglected in our radiative model.

The latitudinal (not shown) and seasonal variation (Fig. 9) of the bias suggests an error related to the calculation of water absorption of at least 1–2 K. This can be due either to an error in the absorption coefficient for water vapor at 11 μm or to a systematic underestimate of water vapor abundance. The latter explanation does not seem correct, especially since Rosen and Salstein (1980) suggest that the NMC water analyses may be biased high by 10%–20%. Our formulation of the water absorption (Roberts et al. 1976) neglected the contribution of weak lines in the absorption spectrum, which underestimates the water vapor absorption by about 30% (Grassl 1974; Barton 1983). This error is equivalent to 1–2 K of the bias (McMillin and Crosby 1984; Barton 1985). Much better calculations of water vapor absorption should be possible (cf., Luther 1984).

The third effect is caused by the difference between "skin" temperature measured by the radiometer and the subsurface temperature measured by the ships, which can be as large as 1 K (Bernstein 1982; Barton 1983; McClain et al. 1985; Barton 1985; Schlussel et al. 1987). Under clear conditions, the "skin" of the

ocean (the uppermost 0.1–1 cm of water) can be slightly cooler than the bulk temperature, but this relation can be altered by wind stirring. The uncertainty in the calibration of the radiometer (fourth effect), needed to account for most of the remaining 1–2 K bias in our results, is similar to other estimates of calibration uncertainties (Njoku 1985).

Miyakoda and Rosati (1982) compared several ship-only, satellite-only, and mixed ship-satellite SST analyses from 1976 and 1977 to their own analysis of ship data and of data from the same NOAA-5 SR that we used. Their overall assessment of the comparison was that the agreement was generally good to within 1–2 K (standard deviation of 1.5 K), with the larger errors occurring in highly cloudy regions. Comparison of our results to their preferred result shows agreement to within the same 1–2 K with a higher standard deviation of 2.5–3 K. In particular, their analysis confirms some of the larger differences between our SSTs and the climatological norm for January 1977: a strong positive

TABLE 3. Comparison of SR SSTs (in parentheses) with SST from Miyakoda and Rosati (1982) in °C.

Location	January	July
50°N, 180°E	3.5 (1.3)	10.0 (9.2)
50°N, 140°W	7.5 (6.8)	9.0 (10.2)
35°N, 150°E	16.5 (13.3)	24.0 (23.7)
35°N, 140°W	17.0 (14.3)	21.0 (20.2)
0°N, 180°E	28.0 (26.3)	29.5 (27.7)
180°E: Diff 50°N to 0°	24.5 (25.0)	19.5 (18.5)
140°W: Diff 50°N to 35°N	9.5 (7.5)	12.0 (10.0)

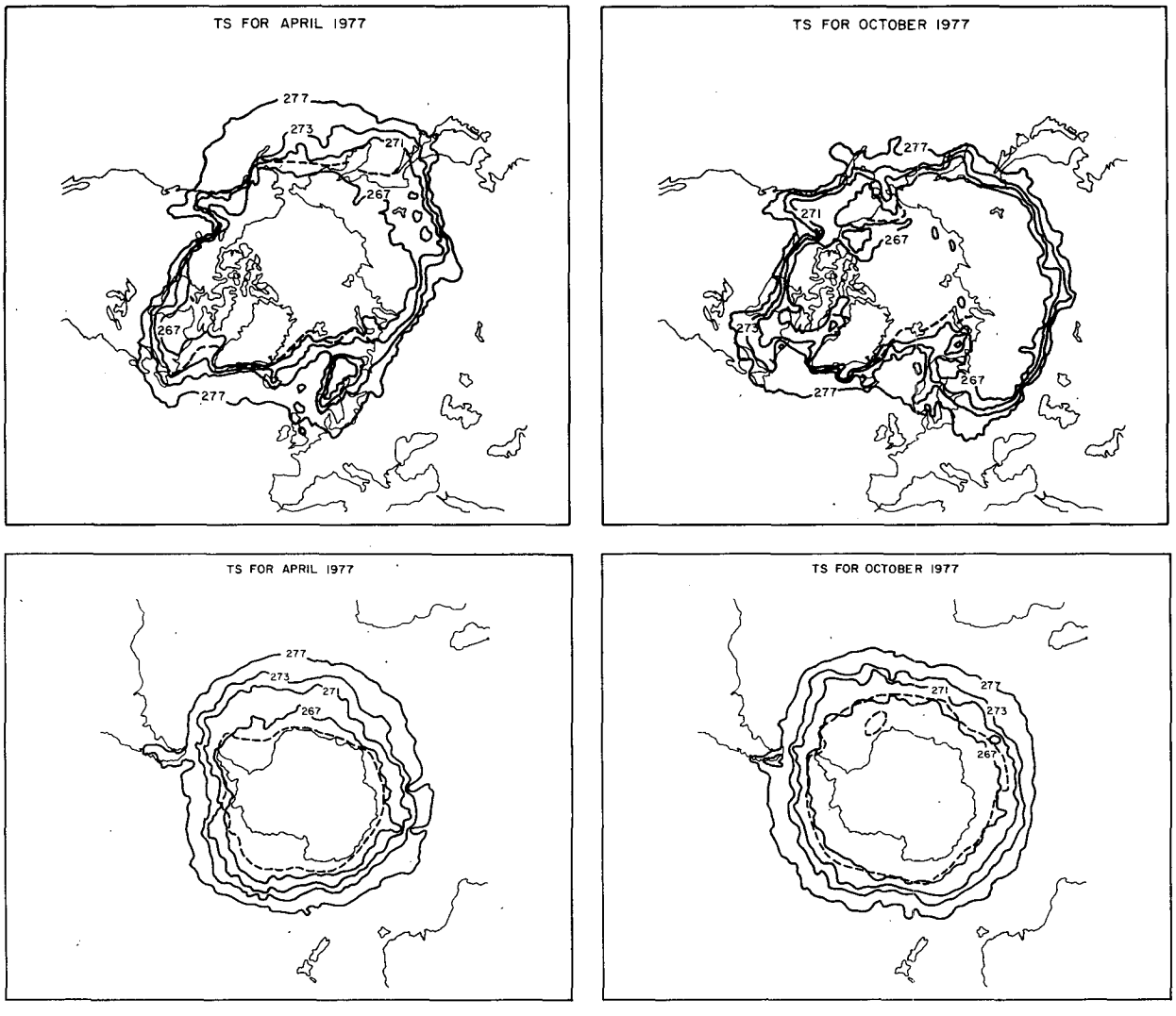

FIG. 10. Comparison of microwave sea ice edges in April and October 1976 (Zwally et al. 1983; Parkinson et al. 1987), shown by the dashed lines, to the surface temperature isotherms deduced from NOAA-5 SR measurements in the Arctic for (a) April 1977 and (b) October 1977 and in the Antarctic for (c) April 1977 and (d) October 1977. The surface temperature contours are labeled. These values have been corrected for the hemispheric mean bias shown in Fig. 9.

anomaly near the Chilean coast, consistent with the ongoing El Niño event, strong positive anomalies throughout the 10°–30°S latitude zone, and a strong negative anomaly in the western equatorial Pacific (little water with SST > 28C). In addition to a comparison of our results with those of Miyakoda and Rosati (1982) at individual locations, we also compared horizontal temperature differences and found agreement to 1–2 K. These comparisons are summarized in Table 3 by showing comparisons of the measured seasonal variations of SST at the specific test sites studied by Miyakoda and Rosati (1982). Figure 15 shows another regional comparison; the SR values shown here have had the January, hemispheric mean bias (Fig. 9a) removed.

Sea ice positions compare favorably with other analyses (as discussed above), but no information is available to verify the surface temperatures retrieved. Figure 10 shows a reasonable correspondence between the 271 K isotherm in April and October 1977 and the microwave ice line position in the Arctic and Antarctic in April and October 1976 (Zwally et al. 1983; Parkinson et al. 1987) near Antarctica. The larger discrepancy for Antarctica in April may be due to significant cloud contamination of our TS values near the ice edge. Since water vapor abundances are very low and ice emissivity is nearly unity (Warren 1982), the expected uncertainty in retrived sea ice surface temperatures is on the order of the synoptic variability of the sea ice surface temperature, which is neglected in this analysis. Variation of sea ice surface temperatures are not well studied, but we estimate from small-scale spatial variations that the uncertainty is ~4 K.

In summary, the uncertainty in the relative SST values (with the bias eliminated), is ~2 K, associated with radiometer noise and uncertainties in atmospheric temperature and water vapor abundances. Figure 11 shows the annual mean variation of SST for 1977 obtained from this analysis. Values in some locations are biased by persistent cloudiness: persistent portions of the ITCZ are in the western Pacific and eastern Indian oceans, near Central America, and off the coast of Guinea and the marine stratus regions off western Africa, the west coast of Australia, off Peru, off the southwest coast of North America, and off Angola/Namibia (the latter two regions are very persistent). Radiometer calibration uncertainties are the largest source of bias, overall.

e. Land surface temperature

Land surface temperatures are more variable because the faster radiative response of the land surface allows diurnal, synoptic, and seasonal variations to have significant amplitude (cf. Idso et al. 1975; Wetzel et al. 1984). The result of the statistical analysis of the satellite data in our method is assumed to represent the monthly

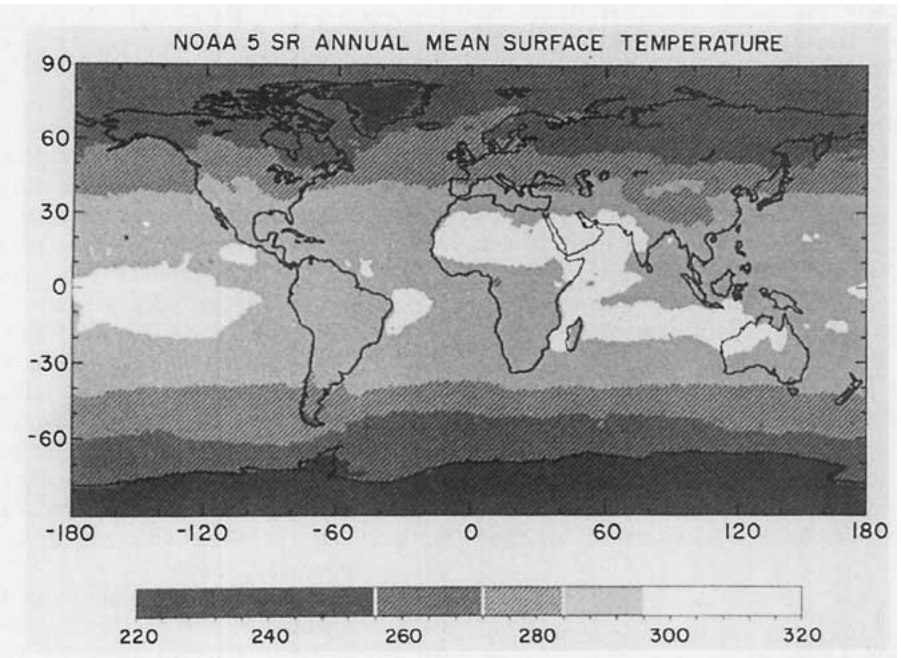

FIG. 11. Geographic distribution of annual mean surface (brightness) temperatures in degrees Kelvin from NOAA-5 SR data from 1977. Values are averaged to 1° resolution and represent the mean values for January, April, July, and October, except at latitudes > 65°W where no value is contributed from the winter months (see Fig. 16). Hash marks divide the grey scale at the annual global mean surface temperature. The values shown on the gray scale include all values that occur.

mean surface temperature at the local time of day corresponding to the satellite overflight. This result is then combined with the synoptic deviations inferred from the NMC analysis dataset to produce a daily surface temperature value at each location at a resolution of 2.5°. Figure 12 shows the histogram of the point-by-point differences between the satellite monthly values and the monthly mean, collocated surface station reports.[2] The distribution of differences is much broader over land, ~5–6 K, and the bias is also larger and more variable with season than for the ocean surface. The same factors contribute to the land bias as for the ocean, with the water vapor effect slightly smaller and the emissivity effect larger (cf. Wetzel et al. 1984).

Emissivities for various surface materials vary between 0.7 and 0.95, with increasing moisture content causing increasing values (Buettner and Kern 1965; Hovis and Callahan 1966; Prabhakara and Dalu 1976). Some geometric variation is also exhibited by desert surfaces (Staylor and Suttles 1986). The geographic variation of land surface emissivity, especially that associated with vegetation variations, increases the dispersion of the differences between the blackbody temperature and the actual surface temperature shown in Fig. 12, but the emissivity effect is actually a bias error that varies with location. Since the *average* emissivity is smaller than for the ocean, a larger bias is also expected (≈2 K).

The equivalent of the "skin" effect for land measurements is that the temperature of the solid surface or vegetation canopy (the "skin") differs from the air temperature at 1–2 m altitude where it is measured by weather stations. Probably the most extreme differences are those that occur in arid regions; Buettner and Kern (1965) report differences in the Sahara ≈10 K over rock surfaces and 15–30 K over sand surfaces. This difference can vary with season (Fig. 12) and time of day (Minnis and Harrison 1984a,b); Idso et al. (1975) report diurnal variations in the "skin"–air temperature difference from 2 to 20 K. Geographic variations are also caused by variations in such factors as the vegetation canopy height and soil moisture (Wetzel et al. 1984). The map of the differences (Fig. 13) shows the expected patterns: larger positive differences in arid regions (e.g., central Asia) than in moist regions and larger positive differences in summer than winter (shown by the shift from a negative to a positive bias). Some of these sources of discrepancy between the satellite and ground data, which can be ≈5–10 K, are not an error

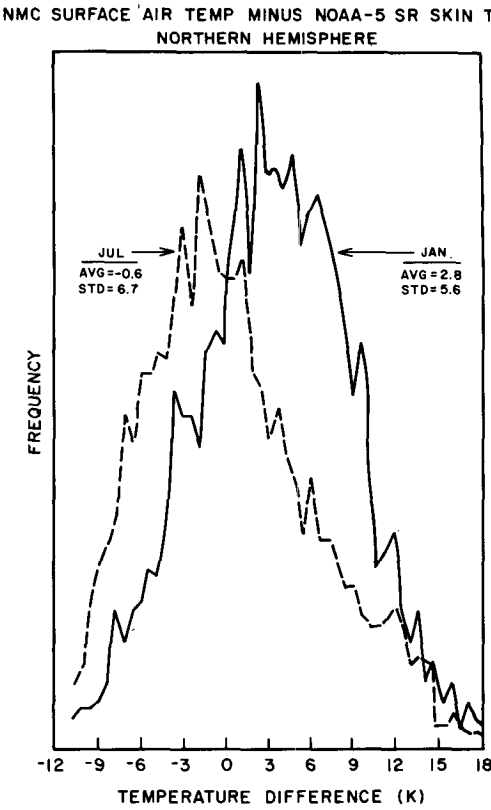

FIG. 12. Distribution of the differences between the monthly mean NMC surface station air temperature reports and the NOAA-5 SR surface (brightness) temperature for January (solid) and July (dashed) 1977 on Northern Hemisphere land surfaces. Only the station report nearest in time to the NOAA-5 overflight time is used in the average. The average and standard deviation of the differences are also shown.

in the satellite analysis, but rather represent a difficulty in validating satellite measurements using conventional surface observations. However, to obtain the "physical" surface temperature from satellite measurements requires corrections for each site to account for these effects. If only the clear sky radiation is desired, then the effective value defined by the satellite measurements can be more accurate, if the same assumptions are used in the retrieval model as in the radiation model.

Several regions of negative bias are also apparent in the tropics in Fig. 13; these represent areas of persistent cloud cover (e.g., the summer monsoon region in India) that contaminate the satellite observations. These areas are also well correlated with bright anomalies in the surface reflectance maps.

The larger and more seasonally variable bias between the average satellite and average station temperatures (shown in Fig. 12) is also produced, partly, by a difference in the samples of time variations included in the two averages. Whereas the station data include measurements from every day in the month—cloudy or clear—the satellite data only include measurements for clear days. This effect also alters the relation between

[2] This surface temperature dataset is obtained from the NMC collection of reports from over 4000 conventional weather stations; averages are produced for the same 2.5° square regions and for the time of day closest to the satellite overpass time. Although these data are used to produce the NMC analysis of surface temperature, there are significant differences between the station report summary and the NMC analysis product (see Ro89), which also contribute to the differences shown in Fig. 12.

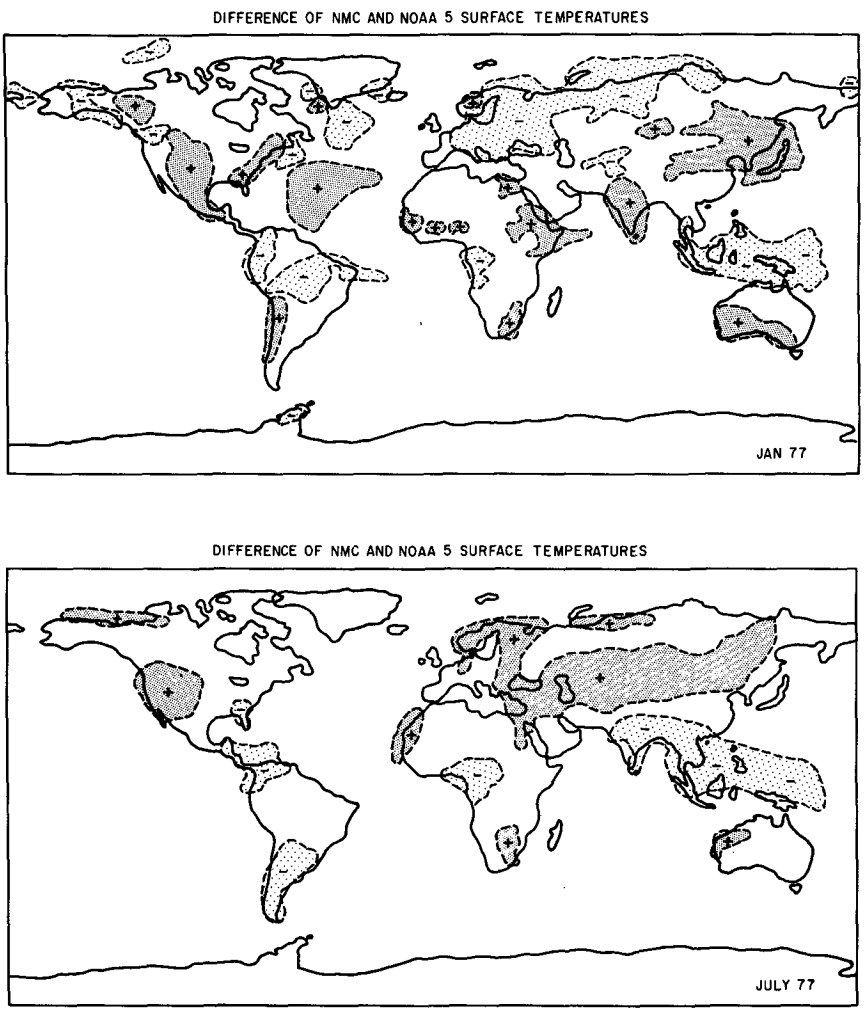

FIG. 13. Geographic distribution of surface temperature differences larger than one standard deviation from the mean difference between the NMC ship and surface station air temperatures and the NOAA-5 SR surface (brightness) temperatures for (a) January and (b) July 1977. The average and standard deviation of the differences used to produce these maps are different for ocean (see Fig. 9) and land (see Fig. 12) and month. Positive values of the difference (heavy shading) indicate that the NOAA-5 values are warmer than the NMC values; negative differences (light shading) indicate that NOAA-5 values are colder. No shading means that the values differ by less than one standard deviation.

the "skin" temperature and the near-surface air temperature. This "clear sky" bias was revealed in daily case studies (Fig. 14) comparing the combined SR and NMC surface temperatures with the station reports at satellite overpass time for a 2-week period in January and July over the United States. The effect showed up as a characteristic pattern of error, such that the station temperatures in cloudy regions are generally warmer (colder) than the satellite temperatures in winter (summer), while adjacent clear regions were in good agreement, i.e., showing only the expected bias caused by the "skin vs air temperature" effect. The seasonal dependence of geographic biases (Fig. 13) is also consistent with the relation that clear days are generally colder (warmer) than the monthly mean in winter (summer).

Case studies comparing surface temperatures retrieved from manually selected cloud-free images with the monthly mean distribution of surface temperatures show overall correspondence to within 5–8 K. Temperatures for 6 specific days were also compared to station reports over the United States to test the combination of SR and NMC data to reproduce the day-to-day surface temperature variations. Figure 15 shows one example with the mean bias removed (a different bias is removed for land and water based on Figs. 9 and 12). As can be seen, most of the large-scale features over land are correctly reproduced by this combination of data.

The seasonal cycle of zonal mean temperatures, which is dominated by land variations, is shown in Fig.

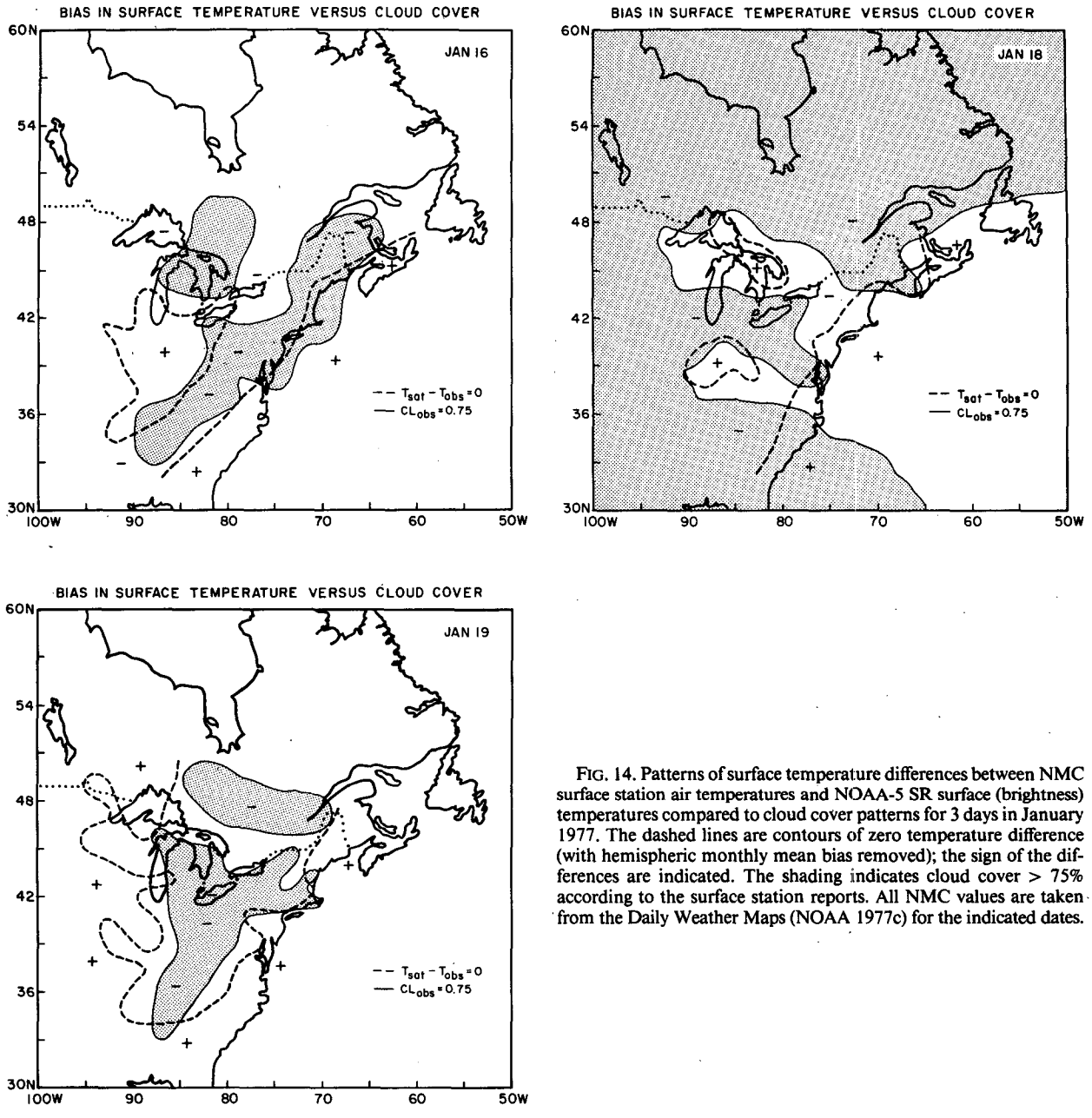

FIG. 14. Patterns of surface temperature differences between NMC surface station air temperatures and NOAA-5 SR surface (brightness) temperatures compared to cloud cover patterns for 3 days in January 1977. The dashed lines are contours of zero temperature difference (with hemispheric monthly mean bias removed); the sign of the differences are indicated. The shading indicates cloud cover > 75% according to the surface station reports. All NMC values are taken from the Daily Weather Maps (NOAA 1977c) for the indicated dates.

16; the geographic patterns of the annual mean values are shown in Fig. 11. Comparison of the geographic and seasonal locations of isotherms (corrected for the bias discussed above) shows good correspondence with the maps shown by Herman and Johnson (1980). As examples: 1) the 278 K isotherm in our January results goes from England to the East Coast of the United States at about 40°N and from near Alaska to Tokyo in the Pacific, whereas the climatology shows a slightly more southern position of this isotherm in the North Pacific; 2) the 278 K isotherm in our Southern Hemisphere results is nearly identical to that shown by Herman and Johnson (1980); 3) the climatology shows a temperature in Greenland in July of about 263 K, whereas our results give a value of 258 K with no bias corrections; and 4) the climatology shows a temperature in Antarctica in January of 243 K compared to our result of 249 K, with no bias corrections.

In summary, the dispersion of the temperature differences and the discrepancies shown in the test cases suggest that this analysis reconstructs the land surface temperatures within about 6 K. The variation of emissivities on land contributes about one-third of this error, whereas time variations seem responsible for much of

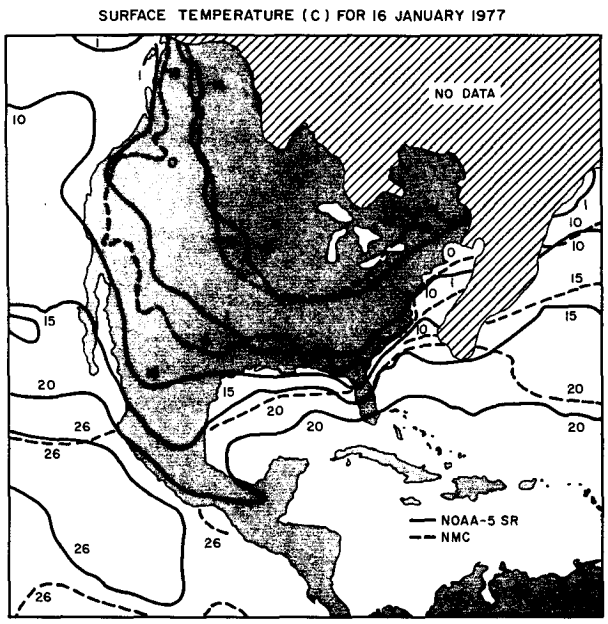

FIG. 15. Comparison of surface temperature for North America from NOAA-5 SR data (solid contours) with NMC surface data (dashed contours). The NOAA-5 SR results combine the monthly mean satellite-measured value with the daily deviations from the monthly mean NMC analysis over land to produce daily values; both the NOAA-5 and NMC values over ocean are monthly means. The NOAA-5 SR surface temperatures have been changed to eliminate the hemispheric, monthly mean bias (see Figs. 9 and 12).

the remainder.[3] Price (1984) estimates retrieval errors of 2–3 K, using a split-window method, when errors caused by regional emissivity variations and calibration uncertainties are neglected. Usually persistent cloudiness causes problems in the same tropical areas mentioned in section 3b and over higher latitude winter continents, particularly northwest North America and northern Europe.

f. General problems

The emphasis of the above comparisons of satellite-derived and surface-measured quantities has been on assessment of regional and global scale sources of error. There are several general sources of uncertainty in such satellite measurements that arise which are not usually discussed in the literature; these difficulties can become very important when attempting to measure small-scale or detailed behavior of surfaces and are the reason for the statistical approach to measuring larger-scale variations used here. These "external" sources of measurement variation are unmeasured atmospheric variations, radiometer performance limitations, navigation "jitter," and classification errors.

Although atmospheric effects at some wavelengths are quite small and corrections can, in principle, be made accurately if atmospheric properties are known, small variations in atmospheric mass (surface pressure) and aerosol content can occur on very short time scales. Thus, even the effect of absorptions by "constant" atmospheric gases will vary slightly and, consequently, the radiances measured by satellites will exhibit very small variations. This "atmospheric noise" can be eliminated if the observation density is high enough in time and space to allow average values to be calculated.

"Instrumental" noise of several varieties also is common in satellite data. In addition to the noise level in the radiometer, some datasets are contaminated by external interference in the telemetry (on-board the spacecraft or in the receiving antenna) and by processing errors on the ground. This type of problem makes analysis schemes that use a single measurement or an extreme value (e.g., minimum albedo or maximum temperature) very risky. Other instrument performance problems can appear in very high resolution measurements or in observations of low contrast or

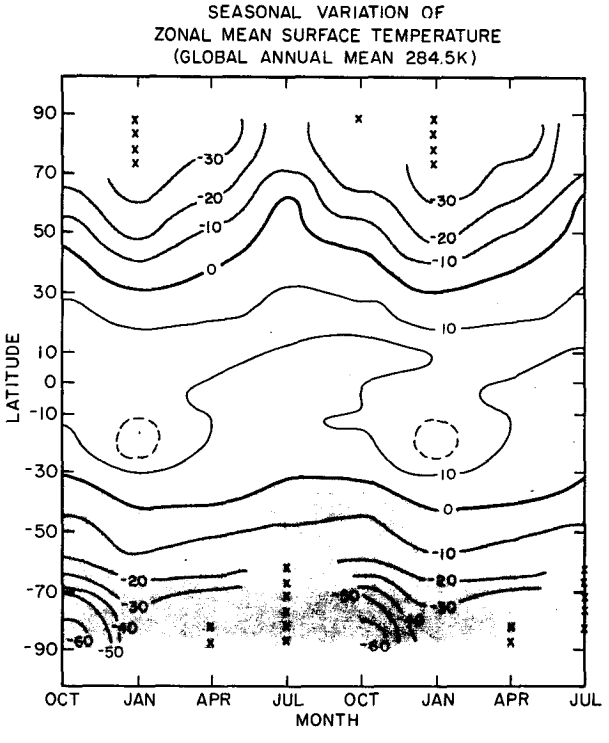

FIG. 16. Seasonal variation of zonal mean surface temperatures from NOAA-5 SR data for January, April, July, and October 1977. Solid contours indicate 10 K intervals in zonal mean as deviations with respect to the annual global mean value; the dashed contour is a deviation of 15 K. Shading indicates negative deviations; x-marks indicate no measurement is available. The 4 monthly values are repeated to produce the seasonal cycles.

[3] Some of our error is produced by the use of the NMC model-analyzed surface temperatures, which do not always agree well with the original observations.

low signal situations. Some radiometers or ground processing systems place (undocumented) limits on observation values that also degrade data quality.

Navigation "jitter" refers to the variation in location of a particular satellite observation caused by uncertainties in spacecraft attitude and instrument pointing. Spurious time variations appear because the locations of the measurements are not actually constant. In certain cases, this uncertainty can lead to errors associated with improper scene classifications; e.g., measurement of surface properties in coastal waters is made difficult by the varying location of the coastline.

The most important classification error is mistaking cloudy conditions for clear. Even a small amount of clouds can significantly alter satellite-measured radiances and the accuracy of surface measurements. Other "classifications" can also be important to study results, such as measurements of certain vegetation types or of snow-covered land, where the accuracy is dependent on the reliability of these identifications.

4. Discussion of results

Although the imaging data from operational weather satellites may not provide the most detail about the properties of the earth's surface, due to limitations of spectral and spatial resolution or calibration, we can already see the advantage of their use for global studies. A systematic and quantitative analysis of satellite data, such as presented here, can give global coverage at relatively high spatial and temporal resolution and provide a comprehensive view of the large-scale patterns of the space and time variations of the surface. The data coverage and density not only allow for verification of the results by exploiting any other available datasets that overlap in space and time, but also allow detection of certain analysis biases by comparisons under widely different conditions. Repeated measurements at each location are particularly important to separating intrinsic variations from measurement errors, as has been illustrated in the case of water vapor effects on surface temperature.

The annual mean surface reflectance and temperature for 1977, averaged over ±60° latitude, are 5% and 288 K, respectively (Table 4). If the polar regions are included (no winter pole results), then these values are 10% and 284.5 K, respectively. Adjustments for the ozone bias in the surface reflectances at high latitudes would increase the global mean surface reflectance value by no more than 1%–2% (see Matthews and Rossow 1987). Adjustment for the emissivity and other biases in the surface temperatures would increase the global mean value by about 3–5 K; however, inclusion of the winter poles would also decrease the global mean surface temperature by 1–2 K, approximately.

These values are the narrowband quantities defined by the NOAA SR instrument; the "true" spectrally integrated values will be different. Broadband surface albedo is expected to be higher, both because of the higher near-IR reflectances of vegetated surfaces (although snow/ice cover can reduce the albedo in the near-IR) and because of the contributions from higher solar and viewing zenith angles in the diurnal average. Other estimates of the global, annual mean surface albedo are about 13%–16% (e.g., Posey and Clapp 1964; Hummel and Reck 1979; Robock 1980). Calibration could change the larger reflectance values, but would not affect the global mean very much because it is dominated by the ocean reflectance, which is in good absolute agreement. Temperatures of the solid/liquid surface obtained from a broadband measurement would probably be close to those inferred from this type of data. To obtain the physical surface temperature, corrections are needed for the spectral variations of the emissivity and the clear sky bias effect. The former correction could increase the mean value by 1–3 K; the latter correction could shift the global annual mean value either way. Averaging over the whole diurnal cycle would probably change this value only slightly, since the temperatures in midmorning (NOAA-5 overflight time) are intermediate in value to the diurnal extremes. Calibration uncertainties can also shift the temperatures by similar amounts. Estimates of the global, annual mean surface *air* temperature give a value near 288 K (Oort 1983); the "skin" temperatures are probably a few degrees Kelvin larger than this value.

The Northern and Southern hemispheres are nearly the same in annual mean temperature (excluding the polar regions), with the Southern Hemisphere being slightly (0.5 K) warmer; but the Northern Hemisphere reflectance is higher by about 4% due to the larger amount of land (Table 4). If the polar regions are included, then the Southern Hemisphere is slightly colder than the Northern Hemisphere in the annual mean; i.e., Antarctica is much colder than the Arctic. Oort (1983) gives an annual mean Southern Hemispheric mean surface temperature about 1 K colder than the

TABLE 4. Summary of annual mean spatial variations of surface properties. Global and hemispheric mean values refer to averages over the lowest 60° of latitude in each hemisphere. (Global mean values in parentheses show the averages over all latitudes, but no winter pole observations are included.) The signs on the hemispheric deviations refer to the Northern and Southern hemispheres, respectively. Values in square brackets are corresponding values for RS from Hummel and Reck (1979) (these are total albedo values) and for TS from Oort (1983).

Quantity	Global mean	Estimated uncertainty	Deviation of mean hemispheric value	rms deviation of zonal mean
RS (%)	5 (10)	3	±2 (0)	3
	[15]	—	[±2]	—
TS (K)	288.3 (284.5)	4	∓0.2	20.7
	[288.0]	—	[±0.6]	—

TABLE 5. Summary of seasonal deviations of the global and hemispheric averages of surface properties from their global annual mean values. The first number in each column is the global mean value or deviation from the global annual mean; the numbers in parentheses are the (Northern/Southern) hemispheric deviations from the global annual mean, respectively. Values in square brackets are corresponding values for RS from Hummel and Reck (1979) (these are total albedo values) and for TS from Oort (1983).

Quantity	Annual mean	Jan	Apr	Jul	Oct
RS (%)	5 (+2/−2)	+1 (+5/−2)	0 (+1/−2)	+2 (0/+3)	0 (0/−1)
	[15 (+1.7/−1.7)]	[+0.4 (+4.1/−3.3)]	—	[−1.6 (−4.7/+1.5)]	—
TS (K)	288.3 (−0.2/+0.2)	−0.6 (−6.7/+5.5)	+0.2 (+0.9/−0.5)	+0.6 (+4.4/−3.2)	−0.2 (+0.6/−1.0)
	[288.0 (+0.6/−0.6)]	[−1.8 (−6.0/+2.2)]	—	[+1.8 (+6.8/−3.2)]	—

Northern Hemisphere value; Hummel and Reck (1978) indicate that the Northern Hemisphere albedo is about 3% larger than the Southern Hemisphere albedo.

The two hemispheres also differ in the amplitude of their seasonal variations (Table 5). Both hemispheres exhibit higher surface reflectances in the winter season because of the effect of the solar zenith angle on the ocean reflectance, of some sea ice in the illuminated parts of the ocean, and of snow cover on land. Ocean reflectance variations dominate the seasonal cycle in the Southern Hemisphere, while snow cover variations dominate in the Northern Hemisphere. Very little snow cover occurs in the Southern Hemisphere, leading to a smaller seasonal amplitude of surface reflectance than for the Northern Hemisphere. Both hemispheres exhibit the lowest mean temperatures in the winter season, but the seasonal amplitude is about 2–3 K larger in the Northern Hemisphere because of the larger amount of land.[4] If the polar regions are included, the differences between the Arctic Ocean (less seasonal variation) and Antarctic continent (more seasonal variation) offset part of the difference in the seasonal amplitude of the lower latitude parts of each hemisphere.

Figure 17 shows the zonal annual mean surface reflectance, and temperature with the seasonal variation amplitude indicated. The variations of surface reflectance among different zones are much larger than the seasonal variation; however, the temperature contrasts are similar in magnitude. The decrease of solar heating with latitude leads to lower temperatures; this effect is offset by the heat transports of the ocean and atmosphere and reinforced by the increase of surface reflectance at high latitudes. Figures 7 and 11 show that this simple picture is made more complicated by the large longitudinal variations of the surface properties at each latitude, which can be as large as the latitudinal contrasts. The large geographic variations are associated primarily with the contrast of land and ocean surface properties. Oceans can be characterized as relatively dark, with little seasonal variation in reflectance, except at high latitudes, and moderately warm with little seasonal variation, except at high latitudes near the sea ice formation region. Land is characterized as relatively bright, with smaller seasonal variations except for snow-covered regions, and either much warmer or colder than the ocean depending on the season.

The geographic patterns shown in Figs. 7 and 11 also reveal additional longitudinal variations associated with well-known changes of topography and vegetation (climate) on land. In particular, the central and northeastern parts of Asia (Siberia and China) exhibit more extreme seasonal variations in surface reflectance and temperature than any other land area (Fig. 18), whereas the low-latitude portions of Africa north of the equator exhibit some of the larger spatial variations of these two surface properties, which are relatively constant in time. The amplitude of seasonal temperature variations is about the same in central Asia as in Antarctica. (if climatology is used for the winter season values, cf. Borisenkov and Dolganov 1982) but the reflectance changes in Antarctica are small. The reflectance contrasts in the Arctic basin in summer are somewhat larger than those in tropical Africa, but the temperature contrasts are small.

The wide variety of surface conditions is summarized in Fig. 19, which shows the frequency distribution of zonal mean surface reflectances and temperatures (in 1° zones) in the annual mean and for each month. These distributions and their seasonal changes, together with the differences shown in Fig. 18, indicate several conclusions about the distribution of climate regimes.

1) The global surface is generally very dark (<10% at 0.6 μm) because it is either covered by water or vegetation; but the land is brighter than water. The major contributions to a higher global mean surface reflectance at 0.6 μm are the African/Arabian deserts, Greenland and Antarctica, and the snow/ice covered portions of North America and Asia in winter (Fig. 7). (Since vegetation is much more reflective in the near-IR portion of the spectrum, total land albedos are actually much higher than ocean albedos. Also, the broadband albedo contrast between vegetated and desert areas and between vegetated and snow-covered areas is not as strong as at 0.6 μm wavelength.)

2) The surface reflectance of most land areas, even

[4] Since the seasonal variation of sea surface temperatures lags the solar seasons by about one month, these results underestimate the seasonal amplitude of SST somewhat.

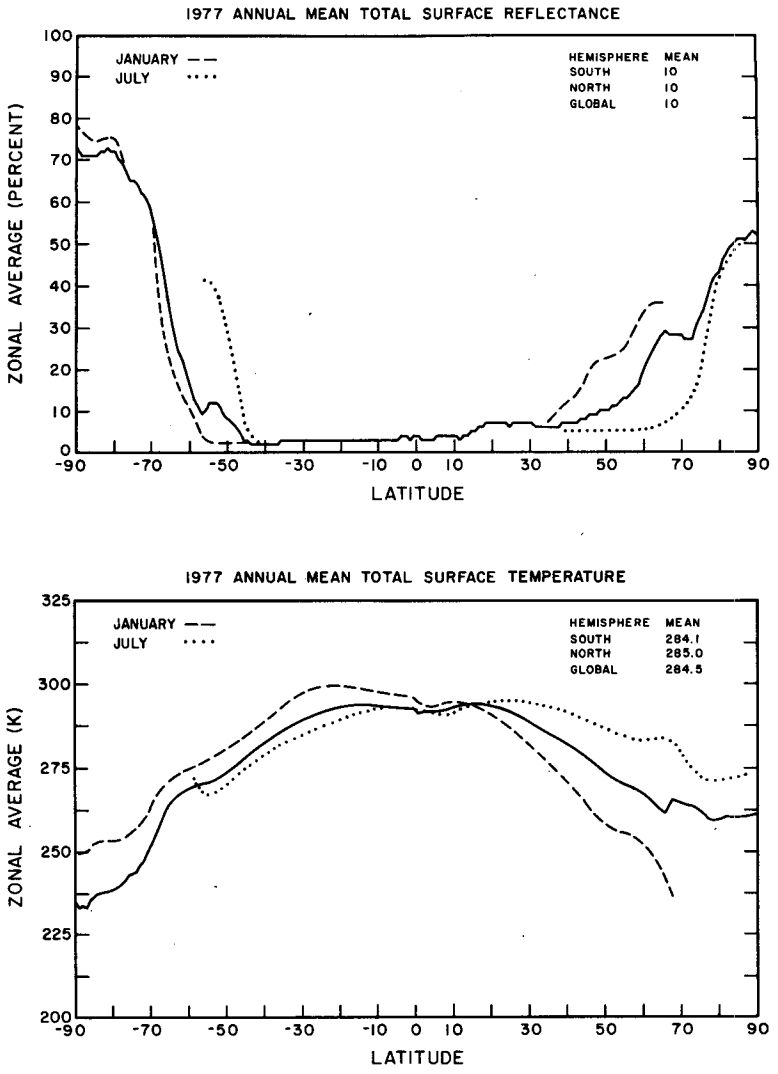

FIG. 17. Annual zonal mean (a) surface reflectance and (b) surface temperature for 1977 from NOAA-5 SR data. The annual mean is shown as a solid line; the dashed line is the January mean and the dotted line is the July mean. Global and hemispheric mean values are also shown.

the bright deserts, is relatively invariant on shorter time scales (cf. Sèze and Rossow 1988) and on seasonal time scales (Fig. 18a), but exhibits significant spatial variations (Fig. 7), consistent with major changes in surface vegetation (Matthews and Rossow 1987). The reflectance of the oceans is invariant in both time and space (Figs. 7 and 18a), except for the seasonal variation associated with solar zenith angle changes at high latitudes. The largest cause of seasonal reflectance variations (at 0.6 μm) in the Northern Hemisphere is snow cover variations. (At near IR wavelengths, where snow is much darker and vegetation much brighter, the seasonal variations of vegetation reflectance may also be an important contribution to seasonal variations.) In the Southern Hemisphere, the largest change comes from the solar zenith angle dependence of water reflectance. Since the location of the sea ice margin is generally near the edge of the illuminated portion of the globe, albedo variation caused by sea ice may be less important than that caused by snow (however, the time lags of snow and ice cover with season differ).

3) The broader surface temperature distributions in Fig. 19 are largely caused by the latitudinal variations of temperature (cf. Fig. 17b); however, significant land/water contrasts at the same latitude do occur (Fig. 11), especially in summer and winter. The spatial scale of surface temperature variations is generally larger than for reflectances (cf. Sèze and Rossow 1988); however, some smaller scale variations can be seen that are associated with topography (Fig. 11). Topographic influ-

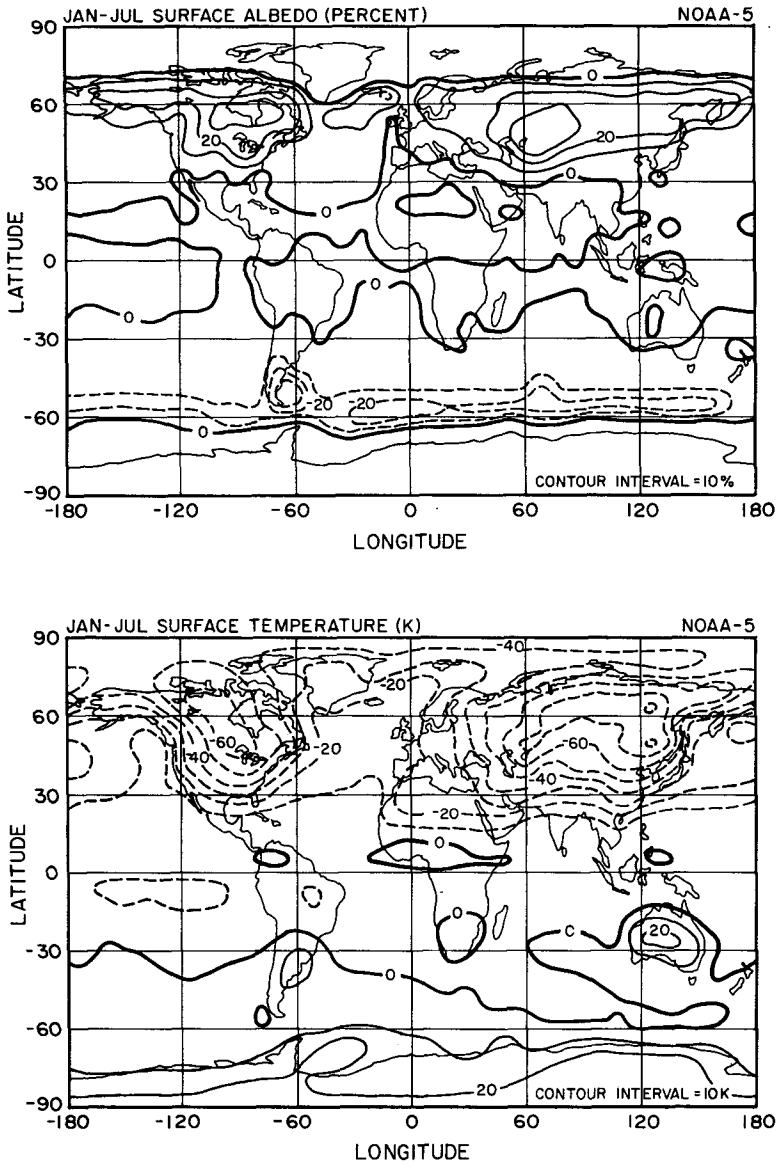

FIG. 18. Geographic distribution of the differences in the January and July 1977 surface (a) visible albedo and (b) temperature from NOAA-5 SR data. The thick solid contour is the zero difference contour; positive differences between January and July are indicated by thin solid contours and negative differences by dashed contours. Land surfaces are assumed to be lambertian to convert reflectances to albedos.

ences on weather patterns are also reflected in large-scale longitudinal variations in land temperature; similar variations across ocean basins reflect the major wind-driven currents (Fig. 11). Time variations of temperature are larger over land than ocean (Fig. 18b) and larger than the spatial variations. The key hot areas of the globe are the African/Arabian deserts and central Asia in summer; the key cold areas are central Asia and Antarctica in winter (Figs. 11 and 18b).

4) The largest seasonal variations in temperature occur on land, particularly at higher latitudes (Fig. 18b). Summer land areas are generally warmer than the ocean at the same latitude; winter land areas are generally colder. Higher latitude oceans also exhibit more seasonal variation in temperature, particularly in the vicinity of the sea ice margin (Fig. 18b).

5) The most variable location on earth, in both surface reflectance (±15%) *and* temperature (±35 K), is central Asia (Fig. 18) (secondarily, central Canada); hence, changes in the average conditions of this one location can be significant in the global seasonal energy balance. Indeed, the strong Asian monsoon cycles are

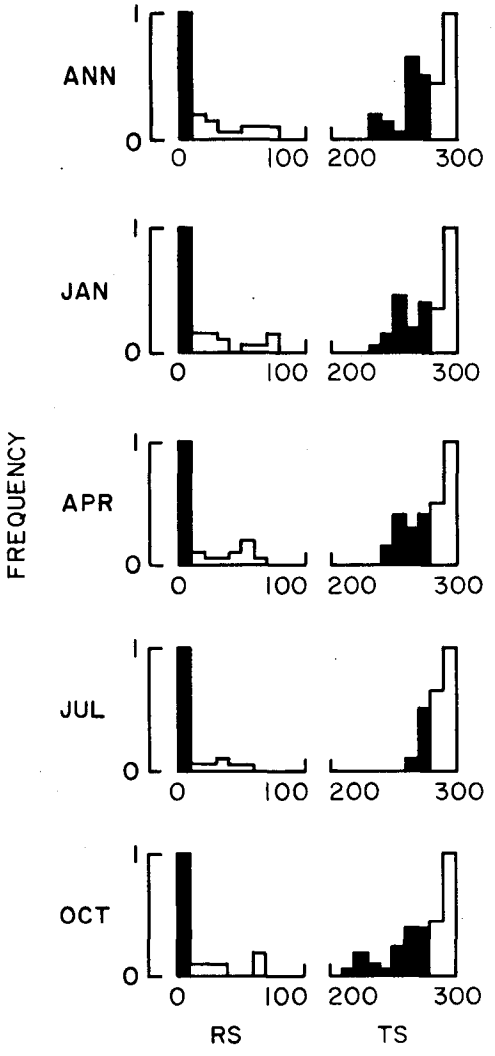

FIG. 19. Distributions of annual and monthly zonal mean values (for 1° zones) of surface visible reflectance (RS from 0 to 100%) and surface temperature (TS from 200 to 300 K). The shading divides each distribution at *approximately* the annual global mean value.

a major anomaly in the global circulation; variations in this part of the world may be a major source of interannual variability in the global circulation.

Even though these data are considered to be coarse resolution compared to those obtained from LANDSAT/SPOT, significant patterns of the land vegetation are revealed that correspond to climate regimes (cf. Matthews and Rossow 1987). In fact, the resolution used here is similar to that employed to study the distribution and variation of vegetation indices (Tucker et al. 1986; Tucker and Sellers 1986). Analysis to remove clouds and other atmospheric effects completely is crucial to detection and interpretation of the small seasonal (and even smaller interannual) variations; cf. the magnitude of seasonal shifts in the distribution of zonal mean values in Fig. 19. In addition, proper treatment of the angular dependence of land surface reflectances, especially the solar zenith angle dependence, is required to avoid the appearance of change being produced by variations in the angular distribution of satellite observations.

The ocean reflectance is quite low at solar wavelengths; however, the presence of suspended particles (usually biota) can produce small changes in the reflectance. Accurate monitoring of ocean "color" also requires strict removal of cloud "contamination" and corrections for atmospheric effects and viewing geometry variations. Since the ocean reflectance is relatively invariant, except for the effects of wind, statistical measures of reflectance should be more reliable than single measurements.

There have not been many *global* studies of snow and ice albedo. Robinson and Kukla (1985) obtained estimates of the maximum albedo of snow covered land; however, no study has been done of the average value as a function of location and the amount of variability exhibited by snow-covered land with different vegetation types and time. A general survey of sea ice albedos also has not been reported. Although there are still problems separating snow/ice from clouds, satellite monitoring of snow/ice cover amounts and albedos with this type of satellite data has been shown to be useful.

In the extreme seasonal months, January and July, the illuminated sea ice extent is not very large. Moreover, the reflectance of open water at large solar zenith angles is quite large. Both these effects decrease the role of sea ice albedo feedback on climate. The illuminated sea ice extent in the transitional months is larger, but this may only serve to affect the timing of the seasonal variations rather than altering the total energy budget. The illuminated extent of snow cover is much larger, primarily in the Northern Hemisphere; thus, snow albedo feedback in northern winter is currently the most important surface albedo feedback (although vegetation changes in the near-IR may be nearly as important). Since the magnitude of the snow brightening is sensitive to the type of vegetation, anthropogenic changes in vegetation can influence the magnitude of this positive feedback on the climate.

Surface temperatures not only indicate the energy balance at the surface that is most important to the biosphere, but also control the other exchange that is crucial, namely evaporation. Monitoring of the high resolution variations of temperature is important to the study of the dynamics of the surface climate system. Satellite data provide the only global view in a short time. In cases where cloudiness is persistent, the statistical variation of the surface temperature variations may still be inferred from the observed patterns. Although some further work is required to convert the satellite-measured parameter into a physical temperature, we have shown that monitoring the temperature *variations* at high resolution is possible.

5. Conclusions

This investigation has highlighted a number of problems that can occur in the analysis of satellite observations of the earth's surface. The most important "problem" for global studies is accommodating the variety of situations encountered into the analysis procedure. The use of single, simple tests to isolate cloud-free conditions, for instance, is not reliable under all circumstances and can produce regionally varying biases in the results. Consequently, the resulting global survey would have variable validity and unknown changes in error sources, making it difficult to monitor global relations over long time periods. Moreover, the magnitude of the seasonal variations exhibited in these results suggests that the investigation of long-term changes will generally require high accuracy measurements that have all extraneous sources of variation removed. These considerations should influence the design of the analysis algorithms.

For example, use of extreme radiances to filter out clouds biases the surface results in a way that is dependent on the amount of both cloud and surface variability. In highly cloudy locations, this approach may produce good results; however, in less cloudy locations this approach can bias the measurement by one to two standard deviations (where the standard deviation is determined by the intrinsic variability of the surface). This bias for surface temperature can be as much as 1–2 K, even over the ocean which has low variability, because of radiometer noise or water vapor variations. The strictness of the tests employed in a cloud algorithm (its sensitivity to clouds) must be determined by the objectives: even a small amount of cloudiness can alter the ocean color or the surface temperatures measured from satellites. On the other hand, if the threshold is too strict, the surface results are biased by cutting off part of their natural distribution. The best approach seems to be to attempt to capture either the actual distribution of the surface variations or some statistic based on the whole distribution, as attempted here.

It is common practice to use only the data that are directly related to the desired parameter in the analysis; however, other data may prove useful in detecting unwanted effects or identifying specific situations that call for a different analysis procedure. In particular, surface analyses need to use all available data to be sure of removing clouds. For example, solar wavelength measurements commonly used to study vegetation should be analyzed together with thermal infrared observations which are more sensitive to thin cirrus overcasts. Thus, the sensitivity to cloudiness of the particular spectral channels studied here recommends their use even for instruments designed for surface studies rather than atmospheric studies.

Investigation of the discrepancies between the satellite-measured values of parameters and those obtained from other sources indicates that, while errors associated with the removal of atmospheric effects are important, they are not predominant. This conclusion would probably not be true at other wavelengths that are more sensitive to the atmosphere. The largest source of error in correcting for atmospheric effects is, however, not the radiative modeling of these effects, but the specification of the atmospheric properties, particularly aerosol and water vapor; hence, monitoring of the atmosphere is also an indispensible part of observing the surface.

The largest source of uncertainty in the retrieved surface properties is that the radiation models do not treat the angle and spectral dependences sufficiently well for complex, heterogeneous surfaces (see Wetzel et al. 1984; Koepke and Kriebel 1987). Variations of the satellite-measured radiances due to these surface attributes cannot yet be completely disentangled from true variations in surface *conditions*. However, the statistical characterization of the behavior of many locations, classified as the same surface type, in a global, long-term dataset, like that obtained here, could be used to develop better models of the interaction of the surface and radiation.

The advantage of satellite observations of the surface, even if the desired quantity is not directly obtained, is that the large-scale space and time patterns are better perceived. Many of the measurement problems discussed here could be alleviated by the complete use of multispectral measurements that allow for a substantial reduction in the number of assumptions that are made in the radiative model, but this is not commonly done. Sea surface temperature and vegetation index data products, for instance, are obtained currently from only two or three spectral channels, even though more spectral channels are available. The combination of a multispectral imaging radiometer and an atmospheric temperature–humidity profiler on one satellite, as on the current NOAA operational weather satellites, presents a good opportunity to exploit this approach by performing a completely self-consistent retrieval of surface, cloud, and atmospheric properties from coincident and simultaneous observations. This type of analysis (similar to that performed here or by Susskind et al. 1984) has not yet been tried using all available spectral channels and instruments directly.

The most difficult regions to study with satellite data are those where cloudiness is unusually persistent or the surface variations are large or occur rapidly compared to those caused by cloudiness. In the former category are parts of tropical ocean and land, particularly in the western Pacific and India during the summer monsoon, and the "polar front" regions of the oceans where the major storm tracks are located. In the latter category are winter continents and the polar regions, where contrast between cloudy and clear conditions is much lower.

Acknowledgments. The complexity of this study required many years of effort on the part of many people. Louis Kanganis carried out the surface temperature comparison study and Kelvin Lee performed additional sensitivity studies on the radiation code and carried out the ocean surface reflectance model and data comparison. Additional analyses of the global distribution of surface properties were carried out by Edward Kinsella with assistance from S. Chan. Discussions with a number of colleagues during this study helped shape its direction and focus: we thank Elaine Matthews, Inez Fung, Rachel Pinker; we also thank David Rind for comments. Photographs were created using software written by Jeff Jonas and hardcopy produced by Patrice Palmer. Graphics were drawn by Lilly DelValle, and final text processing was performed by Elizabeth Devine. Support was provided by the NASA Climate Program managed by Robert Schiffer.

REFERENCES

Alexander, R. C., and R. L. Mobley, 1976: Monthly average sea surface temperatures and ice-pack limits on a 1° global grid. *Mon. Wea. Rev.*, **104,** 143–148.

Andreas, E. L., and S. F. Ackley, 1982: On the differences in ablation seasons of Arctic and Antarctic sea ice. *J. Atmos. Sci.*, **39,** 440–447.

Barnett, T. P., 1984: Long-term trends in surface temperature over the oceans. *Mon. Wea. Rev.*, **12,** 303–312.

Barry, R. G., 1983: Arctic ocean ice and climate: Perspectives on a century of polar research. *Ann. Assoc. Amer. Geogr.*, **73,** 485–501.

——, 1985: Snow and ice data. *Paleoclimate Data Analysis and Modeling,* A. D. Hecht, Ed., John Wiley and Sons, 259–290.

——, 1986: The sea ice data base. *The Geophysics of Sea Ice,* N. Untersteiner, Ed., Plenum Publ., 1099–1134.

——, A. Henderson-Sellers and K. P. Shine, 1984: Climate sensitivity and the marginal cryosphere. *Climate Processes and Climate Sensitivity,* J. Hansen and T. Takahashi, Eds., *Geophys. Monogr.*, **29,** Amer. Geophys. Union, 221–237.

Barton, I. J., 1983: Dual channel satellite measurements of sea surface temperature. *Quart. J. Roy. Meteor. Soc.*, **109,** 365–378.

——, 1985: Transmission model and ground truth investigation of satellite-derived sea surface temperatures. *J. Climate Appl. Meteor.*, **24,** 508–516.

Bernstein, R. L., 1982: Sea surface temperature estimation using the NOAA-6 satellite Advanced Very High Resolution Radiometer. *J. Geophys. Res.*, **87,** 9455–9465.

Birnie, R. V., 1986: Pixel-mixing effects and their significance to identifying snow condition from LANDSAT MSS data. *Int. J. Remote Sens.*, **7,** 845–853.

Borisenkov, E. P., and L. V. Dolganov, 1982: Some results of climatic generalization of meteorological observations in the Antarctic. *J. Geophys. Res.*, **87,** 9653–9666.

Bowman, K. P., and A. J. Krueger, 1985: A global climatology of total ozone from the NIMBUS 7 Total Ozone Mapping Spectrometer. *J. Geophys. Res.*, **90,** 7967–7976.

Brennan, B., and W. Bandeen, 1970: Anisotropic reflectance characteristics of natural earth surfaces. *Appl. Opt.*, **9,** 405–412.

Brest, C. L., 1987: Seasonal albedo of an urban/rural landscape from satellite observations. *J. Climate Appl. Meteor.*, **26,** 1169–1187.

——, and S. N. Goward, 1987: Deriving surface albedo from narrow band satellite data. *Int. J. Remote Sens.*, **8,** 351–367.

Briegleb, B. P., P. Minnis, V. Ramanathan and E. Harrison, 1986: Comparison of regional clear-sky albedoes inferred from satellite observations and model computations. *J. Climate Appl. Meteor.*, **25,** 214–226.

Buettner, K. J. K., and C. D. Kern, 1965: The determination of infrared emissivities of terrestrial surfaces. *J. Geophys. Res.*, **70,** 1329–1337.

Bunting, J. T., and R. P. d'Entremont, 1982: Improved cloud detection utilizing Defense Meteorological Satellite near infrared measurements. AFGL-TR-82-0027, *Environ. Res. Papers,* No. 765, US Air Force Geophysical Laboratory, Hanscomb AFB, 91 pp.

Buriez, J. C., B. Bonnel and Y. Fouquart, 1986: Theoretical and experimental sensitivity study of the derivation of the solar irradiance at the earth's surface from satellite data. *Beitr. Phys. Atmos.*, **59,** 263–281.

Carroll, J. J., and B. W. Fitch, 1981: Effects of solar elevation and cloudiness on snow albedo at the South Pole. *J. Geophys. Res.*, **86,** 5271–5276.

Carsae, F. D., 1982: Arctic sea ice distribution at end of summer 1973–1976 from satellite microwave data. *J. Geophys. Res.*, **87,** 5809–5835.

Castagne, N., P. Le Borgne, J. LeVourch and J-P. Olry, 1986: Operational measurement of sea surface temperatures at CMS Lannion from NOAA-7 AVHRR data. *Int. J. Remote Sens.*, **7,** 953–984.

Chester, D., W. D. Robinson and L. W. Uccellini, 1987: Optimized retrievals of precipitable water from the VAS "split window." *J. Climate Appl. Meteor.*, **26,** 1059–1066.

Comiso, J. C., and H. J. Zwally, 1982: Antarctic sea ice concentrations inferred from NIMBUS 5 ESMR and LANDSAT imagery. *J. Geophys. Res.*, **87,** 5836–5844.

Conlan, E. F., 1973: Operational products from ITOS scanning radiometer data. NOAA Tech. Memo., NESS 52, U.S. Department of Commerce, Washington, DC, 57 pp.

Coulson, K. L., and D. W. Reynolds, 1971: The spectral reflectance of natural surfaces. *J. Appl. Meteor.*, **19,** 1285–1295.

——, G. M. Bouricius and E. L. Gray, 1965: Optical reflection properties of natural surfaces. *J. Geophys. Res.*, **70,** 4601–4611.

Courel, M. F., R. S. Kandel and S. I. Rasool, 1984: Surface albedo and the Sahel drought. *Nature,* **307,** 528–531.

Cutten, D. R., 1985: Atmospheric broadband transmission measurements and predictions in the 8–13 μm window: Influence of water continuum absorption errors. *Appl. Opt.*, **24,** 1085–1087.

Deering, D. W., and T. F. Eck, 1987: Atmospheric optical depth effects on angular anisotropy of plant canopy reflectance. *Int. J. Remote Sens.*, **8,** 893–916.

Dewey, K. F., 1987: Satellite-derived maps of snow cover frequency for the Northern Hemisphere. *J. Climate Appl. Meteor.*, **26,** 1210–1229.

Dey, B., and O. S. R. U. Bhanu Kumar, 1984: Reply. *J. Climate Appl. Meteor.*, **23,** 343–344.

Dirmhirn, I., and F. D. Eaton, 1975: Some characteristics of the albedo of snow. *J. Appl. Meteor.*, **14,** 375–379.

Duggin, M. J., 1985: Factors limiting the discrimination and quantification of terrestrial features using remotely sensed radiance. *Int. J. Remote Sens.*, **6,** 3–27.

Eaton, F. D., and I. Dirmhirn, 1979: Reflected irradiance indicatrices of natural surfaces and their effect on albedo. *Appl. Opt.*, **18,** 994–1008.

Esaias, W. E., G. C. Feldman, C. R. McClain and J. A. Elrod, 1986: Monthly satellite-derived phytoplankton pigment distribution for the North Atlantic Ocean basin. *Eos,* **67,** 835–837.

FAO, 1972: *Atlas of the Living Resources of the Sea.* United Nations FAO, Department of Fisheries, Rome.

Fortuna, J. F., and L. N. Hambrick, 1974: The operation of the NOAA polar satellite system. NOAA Tech. Memo., NESS 60, U.S. Department of Commerce, Washington, DC, 127 pp.

Gates, W. L., and A. B. Nelson, 1975: A new (revised) tabulation of the Scripps topography on a 1° global grid. Part I: Terrain heights. Rep. R-1276-1-ARPA, Rand Corp., Santa Monica, 132 pp.

Grassl, H., 1974: Influence of different absorbers in the window region on radiative cooling (and on surface temperature determination). *Beitr. Phys. Atmos.*, **47**, 1–13.

Grenfell, T. C., and G. A. Maykut, 1977: The optical properties of ice and snow in the Arctic basin. *J. Glaciol.*, **18**, 445–463.

——, and D. K. Perovich, 1984: Spectral albedos of sea ice and incident solar irradiance in the southern Beaufort Sea. *J. Geophys. Res.*, **89**, 3573–3580.

Gruber, A., 1977: Determination of the Earth-atmosphere radiation budget from NOAA satellite data. NOAA Tech. Rep., NESS 76, U.S. Department of Commerce, Washington, DC, 28 pp.

Herman, G. F., and W. T. Johnson, 1980: Arctic and Antarctic climatology of a GLAS general circulation model. *Mon. Wea. Rev.*, **108**, 1974–1991.

Hilsenrath, E., and B. M. Schlesinger, 1981: Total ozone seasonal and interannual variations derived from the 7 year NIMBUS-4 BUV data set. *J. Geophys. Res.*, **86**, 12 087–12 096.

——, D. F. Heath and B. M. Schlesinger, 1979: Seasonal and interannual variations in total ozone revealed by the NIMBUS 4 Backscattered Ultraviolet Experiment. *J. Geophys. Res.*, **84**, 6969–6979.

Ho, D., A. Asem and P. Y. Deschamps, 1986: Atmospheric correction for the sea surface temperature using NOAA-7 AVHRR and METEOSAT-2 infrared data. *Int. J. Remote Sens.*, **17**, 1323–1333.

Holben, B., 1986: Characteristics of maximum-value composite images from temporal AVHRR data. *Int. J. Remote Sens.*, **7**, 1417–1434.

——, and R. S. Fraser, 1984: Red and near-infrared sensor response to off-nadir viewing. *Int. J. Remote Sens.*, **15**, 145–160.

——, D. Kimes and R. S. Fraser, 1986: Directional reflectance response in AVHRR red and near-IR bands for three cover types and varying atmospheric conditions. *Remote Sens. Environ.*, **19**, 213–236.

Hovis, W. A., and W. R. Callahan, 1966: Infrared reflectance spectra of igneous rocks, tuffs, and red sandstone from 0.5 to 22 μm. *J. Opt. Soc. Am.*, **56**, 639–643.

Hummel, J. R., and R. A. Reck, 1979: A global surface albedo model. *J. Appl. Meteor.*, **18**, 239–253.

Idso, S. B., T. J. Schmugge, R. D. Jackson and R. J. Reginato, 1975: The utility of surface temperature measurements for the remote sensing of surface soil water status. *J. Geophys. Res.*, **80**, 3044–3049.

Jacobowitz, H., and A. Gruber, 1975: Calibration of the visible channel of the NOAA 2 scanning radiometer. *Abstracts Second Conference on Atmospheric Radiation*, Arlington, Amer. Meteor. Soc., 67.

Justus, C. G., and M. V. Paris, 1985: A model for solar spectral irradiance and radiance of the bottom and top of a cloudless atmosphere. *J. Climate Appl. Meteor.*, **24**, 193–205.

Kaufman, Y. J., 1987: The effect of subpixel clouds on remote sensing. *Int. J. Remote Sens.*, **8**, 839–857.

Kimes, D. S., 1983: Dynamics of directional reflectance factor distributions for vegetation canopies. *Appl. Opt.*, **22**, 1364–1372.

——, J. S. Smith and K. J. Ranson, 1980: Vegetation reflectance measurements as a function of solar zenith angle. *Photogramm. Eng. Remote Sens.*, **46**, 1563–1573.

——, P. J. Sellers and W. W. Newcomb, 1987: Hemispherical reflectance variations of vegetation canopies and implications for global and regional energy budget studies. *J. Climate Appl. Meteor.*, **26**, 959–972.

Kistler, R. E., and D. F. Parrish, 1982: Evolution of the NMC data assimilation system: September 1978–January 1982. *Mon. Wea. Rev.*, **110**, 1335–1346.

Koepke, P., and K. T. Kreibel, 1987: Improvements in the shortwave cloud-free radiation budget accuracy. Part I: Numerical study including surface anisotropy. *J. Climate Appl. Meteor.*, **26**, 374–395.

Kondratyev, K. Ya., 1969: *Radiation in the Atmosphere.* International Geophysics Series, Vol. 12, Academic Press, 912 pp.

——, 1973: *Radiation Characteristics of the Atmosphere and the Earth's Surface.* Amerind Publ., 580 pp.

Kriebel, K. T., 1978: Measured spectral bidirectional reflection properties of four vegetated surfaces. *Appl. Opt.*, **17**, 253–259.

——, 1979: Albedo of vegetated surfaces: Its variability with differing irradiances. *Remote Sens. Environ.*, **8**, 283–290.

Kuhn, M., and L. Siogas, 1978: Spectroscopic studies at McMurdo, South Pole, and Siple stations during the austral summer 1977–78. *Antarct. J. US.*, **13**, 178–179.

Kukla, G., and D. Robinson, 1980: Annual cycle of surface albedo. *Mon. Wea. Rev.*, **108**, 56–68.

——, and ——, 1981: Climate value of operational snow and ice charts. Glaciological Data Rep. GD-11, 103–119.

Lamb, H. H., 1972: *Climate: Present, Past and Future. Vol. I: Fundamentals and Climate Now.* Methuen, 613 pp.

LaViolette, P., and P. Chabot, 1969: A method of eliminating cloud interference in satellite studies of sea surface temperature. *Deep-Sea Res.*, **16**, 535–548.

Le Marshall, J. F., and A. J. Schreiner, 1985: Limb effects in satellite temperature sounding. *J. Climate Appl. Meteor.*, **24**, 287–290.

Luther, F. M., 1984: *The Intercomparison of Radiation Codes in Climate Models, Longwave Clear-sky Calculations.* World Climate Research Programme, WCP-93, World Meteorological Organization, 37 pp.

Masaki, G. T., 1972 (rev 1976): *The Wolf Plotting and Contouring Package.* GSFC Computer Program Lib. #A00227, Computer Sciences Corporation, NASA Goddard Space Flight Center, 187 pp.

Matthews, E., 1983: Global vegetation and land use: New high resolution data bases for climate studies. *J. Climate Appl. Meteor.*, **22**, 474–487.

——, 1985: Atlas of archived vegetation, land-use and seasonal albedo data bases. NASA Tech. Memo. 86199, 53 pp.

——, and W. B. Rossow, 1987: Regional and seasonal variations of surface reflectance from satellite observations at 0.6 μm. *J. Climate Appl. Meteor.*, **26**, 170–202.

Maul, G., 1981: Application of GOES visible-infrared data to quantifying mesoscale ocean surface temperature. *J. Geophys. Res.*, **86**, 8007–8021.

——, and M. Sidran, 1973: Atmospheric effects on ocean surface temperature sensing from NOAA satellite scanning radiometer. *J. Geophys. Res.*, **78**, 1909–1916.

——, P. W. de Witt, A. Yanaway and S. R. Baig, 1978: Geostationary satellite observations of Gulf Stream meanders: Infrared measurements and time series analysis. *J. Geophys. Res.*, **83**, 6123–6135.

McClain, E. P., W. G. Pichel and C. C. Walton, 1985: Comparative performance of AVHRR-based multichannel sea surface temperatures. *J. Geophys. Res.*, **90**, 11 587–11 601.

McGuffie, K., and A. Henderson-Sellers, 1986: Illustration of the influence of shadowing on high latitude information derived from satellite imagery. *Int. J. Remote Sens.*, **7**, 1359–1365.

McMillin, L. M., and D. S. Crosby, 1984: Theory and validation of the multiple window sea surface temperature technique. *J. Geophys. Res.*, **89**, 3655–3662.

McPherson, R. D., K. H. Bergman, R. E. Kistler, G. E. Rasch and D. S. Gordon, 1979: The NMC operational global data assimilation system. *Mon. Wea. Rev.*, **107**, 1445–1461.

Minnett, P. J., J. R. Eyre and R. W. Pescod, 1987: The variability of the North Atlantic marine atmosphere and its relevance to remote sensing. *Int. J. Remote Sens.*, **8**, 871–880.

Minnis, P., and E. F. Harrison, 1984a: Diurnal variability of regional cloud and clear sky radiative parameters derived from GOES data. Part I: Analysis method. *J. Climate Appl. Meteor.*, **23**, 993–1011.

——, and ——, 1984b: Diurnal variability of regional cloud and clear sky radiative parameters derived from GOES data. Part II: November 1978 cloud distributions. *J. Climate Appl. Meteor.*, **23**, 1012–1031.

Miyakoda, K., and A. Rosati, 1982: The variation of sea surface

temperature in 1976 and 1977. 1: Data analysis. *J. Geophys. Res.*, **87**, 5667–5680.

NAS/NRC, 1983: *Toward an International Geosphere-Biosphere Program.* National Research Council Workshop Rep., National Academy Press, Washington, DC, 81 pp.

Njoku, E. G., 1985: Satellite-derived sea surface temperature: Workshop comparisons. *Bull. Amer. Meteor. Soc.*, **66**, 274–281.

NOAA, 1977a: *Environmental Satellite Imagery.* January, April, July, October 1977. NOAA/NESS Environmental Data Service, National Oceanic and Atmospheric Administration, U.S. Department of Commerce, Washington, DC.

——, 1977b: *Northern Hemisphere Average Snow and Ice Boundaries.* 3 January 1977–2 January 1978. NOAA/NESS Synoptic Analysis Section, National Oceanic and Atmospheric Administration, U.S. Department of Commerce, Washington, DC.

——, 1977c: *Daily Weather Maps, Weekly Series.* National Oceanic and Atmospheric Administration, U.S. Department of Commerce, Washington, DC.

——, 1984: *Oceanographic Monthly Summary: Eastern-Western Arctic Sea Ice Edge Climatology.* J. Wartha-Clark, Ed., National Oceanic and Atmospheric Administration, U.S. Department of Commerce, Washington, DC, 52 pp.

Norton, C. C., F. R. Mosher and B. Hinton, 1979: An investigation of surface albedo variations during the recent Sahel drought. *J. Appl. Meteor.*, **18**, 1252–1262.

Oort, A. H., 1983: *Global Atmospheric Circulation Statistics, 1958–1973.* NOAA Professional Pap. 14, NOAA GFDL, U.S. Department of Commerce, U.S. Government Printing Office, Washington, DC, 180 pp.

Oxford World Atlas, 1973: S. G. Cohen, Ed., Oxford University Press, 190 pp.

Parkinson, C. L., J. C. Comiso, H. J. Zwally, D. J. Cavalieri, P. Gloersen and W. J. Campbell, 1987: *Arctic Sea Ice, 1973–1976: Satellite Passive-Microwave Observations.* NASA SP-489, National Aeronautical and Space Administration, Washington, DC, 296 pp.

Payne, R. E., 1972: Albedo of the sea surface. *J. Atmos. Sci.*, **29**, 959–970.

Pinker, R. T., 1985: Determination of surface albedo from satellites. *Adv. Space Res.*, **5**, 333–343.

——, and J. A. Ewing, 1987: Simulations of the GOES visible sensor to changing surface and atmospheric conditions. *J. Geophys. Res.*, **92**, 4001–4009.

Pinty, B., and G. Szejwach, 1985: A new technique for inferring surface albedo from satellite observations. *J. Climate Appl. Meteor.*, **24**, 741–750.

Posey, J. W., and P. F. Clapp, 1964: Global distribution of normal surface albedo. *Geofis. Int.*, **4**, 33–48.

Prabhakara, C., and G. Dalu, 1976: Remote sensing of the surface emissivity at 9 μm over the globe. *J. Geophys. Res.*, **81**, 3719–3724.

Price, J. C., 1984: Land surface temperature measurements from the split window channels of the NOAA 7 Advanced Very High Resolution Radiometer. *J. Geophys. Res.*, **89**, 7231–7237.

Roberts, R. E., J. E. A. Selby and L. M. Biberman, 1976: Infrared continuum absorption by atmospheric water vapor in the 8–12 μm window. *Appl. Opt.*, **15**, 2085–2090.

Robinson, D. A., and G. Kukla, 1985: Maximum surface albedo of seasonally snow-covered lands in the northern hemisphere. *J. Climate Appl. Meteor.*, **24**, 402–411.

Robock, A., 1980: The seasonal cycle of snow cover, sea ice, and surface albedo. *Mon. Wea. Rev.*, **108**, 267–285.

——, and D. Kaiser, 1985: Satellite-observed reflectance of snow and clouds. *Mon. Wea. Rev.*, **113**, 2023–2029.

Ropelewski, C. F., A. Robock and M. Matson, 1984: Comments on "An apparent relationship between Eurasian spring snow cover and the advance period of the Indian Summer Monsoon." *J. Climate Appl. Meteor.*, **23**, 341–342.

Rosen, R. D., and D. A. Salstein, 1980: A comparison between circulation statistics computed from conventional data and NMC Hough analyses. *Mon. Wea. Rev.*, **108**, 1226–1247.

Rossow, W. B., F. Mosher, E. Kinsella, A. Arking, M. Desbois, E. Harrison, P. Minnis, E. Ruprecht, G. Sèze, C. Simmer and E. Smith, 1985: ISCCP cloud algorithm intercomparison. *J. Climate Appl. Meteor.*, **24**, 877–903.

——, L. C. Garder, and A. A. Lacis, 1989: Global, seasonal cloud variations from satellite radiance measurements. 1. Sensitivity of analysis. *J. Climate*, **2**, (in press).

Salomonson, V. V., and W. E. Marlatt, 1968: Anisotropic solar reflectance over white sand, snow and stratus clouds. *J. Appl. Meteor.*, **7**, 475–483.

Saunders, R. W., 1986: An automated scheme for the removal of cloud contamination from AVHRR radiances over western Europe. *Int. J. Remote Sens.*, **7**, 867–886.

——, and K. T. Kriebel, 1987: An improved method for detecting clear sky and cloudy radiances from AVHRR data. *Int. J. Remote Sens.*, **9**, 123–150.

Scharfen, G., R. G. Barry, D. A. Robinson, G. Kukla and M. C. Serreze, 1987: Large-scale patterns of snow melt on Arctic sea ice mapped from meteorological satellite imagery. *Ann. Glaciol.*, **9**, 1–6.

Schluessel, P., H-Y. Shin, W. J. Emery and H. Grassl, 1987: Comparison of satellite-derived sea surface temperatures with in situ skin measurements. *J. Geophys. Res.*, **92**, 2859–2874.

Scialdone, J., and A. Robock, 1987: Comparison of northern hemisphere snow cover data sets. *J. Climate Appl. Meteor.*, **26**, 53–68.

Sèze, G., and M. Desbois, 1987: Cloud cover analysis from satellite imagery using spatial and temporal characteristics of the data. *J. Climate Appl. Meteor.*, **26**, 287–303.

——, and W. B. Rossow, 1988: Time-cumulated visible and infrared radiance histograms used as a descriptor of cloud cover. *J. Appl. Meteor.*, (submitted).

Shenk, W. F., and V. V. Salomonson, 1972: A multispectral technique to determine sea surface temperature using NIMBUS 2 data. *J. Phys. Oceanogr.*, **2**, 157–167.

Singh, S. M., 1984: Removal of atmospheric effects on a pixel by pixel basis from the thermal infrared data from instruments on satellites. The Advanced Very High Resolution Radiometer (AVHRR). *Int. J. Remote Sens.*, **5**, 161–183.

Smith, W. L., P. Rao, R. Koffler and W. Curtis, 1970: The determination of sea surface temperature from satellite high resolution infrared window radiation measurements. *Mon. Wea. Rev.*, **98**, 604–611.

——, H. M. Woolf, C. M. Hayden, D. Q. Wark and L. M. McMillin, 1979: The TIROS-N Operational Vertical Sounder. *Bull. Amer. Meteor. Soc.*, **60**, 117–118.

Staylor, W. F., and J. T. Suttles, 1986: Reflection and emission models for deserts derived from NIMBUS-7 ERB Scanner measurements. *J. Climate Appl. Meteor.*, **25**, 196–202.

Streten, N. A., and D. J. Pike, 1980: Characteristics of the broadscale Antarctic sea ice extent and the associated atmospheric circulation 1972–1977. *Arch. Meteor. Geophys. Bioklim.*, **29**, 279–299.

Sturman, A. P., and M. R. Anderson, 1985: A comparison of Antarctic sea ice data sets and inferred trends in ice area. *J. Climate Appl. Meteor.*, **24**, 275–280.

Susskind, J., J. Rosenfield, D. Reuter and M. T. Chahine, 1984: Remote sensing of weather and climate parameters from HIRS2/MSU on TIROS-N. *J. Geophys. Res.*, **89**, 4677–4697.

Takashima, T., and Y. Takayama, 1981: Emissivity and reflectance of the model sea surface for the use of AVHRR data of NOAA satellites. *Pap. Meteor. Geophys.*, **32**, 267–274.

Tanaka, M., and T. Nakajima, 1977: Effects of oceanic turbidity and index of refraction of hydrosols on the flux of solar radiation in the atmosphere-ocean system. *J. Quant. Spectrosc. Radiat. Transfer*, **18**, 93–111.

Toon, O. B., and J. B. Pollack, 1976: A global average model of

atmospheric aerosols for radiative transfer calculations. *J. Appl. Meteor.*, **15**, 225–246.

Tucker, C. J., and P. J. Sellers, 1986: Satellite remote sensing of primary production. *Int. J. Remote Sens.*, **7**, 1395–1416.

——, I. Y. Fung, C. D. Keeling and R. H. Gammon, 1986: Relationship between atmospheric CO_2 variations and a satellite-derived vegetation index. *Nature*, **319**, 195–199.

Vukovitch, F., 1971: Detailed sea surface temperature analysis utilizing NIMBUS HRIR data. *Mon. Wea. Rev.*, **99**, 812–817.

Wadhams, P., 1981: The ice cover in the Greenland and Norwegian seas. *Rev. Geophys. Space Phys.*, **19**, 345–393.

Walsh, J. E., and C. M. Johnson, 1979: An analysis of Arctic sea ice fluctuations, 1953–77. *J. Phys. Oceanogr.*, **9**, 580–591.

Walton, C., 1985: Satellite measurement of sea surface temperature in the presence of volcanic aerosols. *J. Climate Appl. Meteor.*, **24**, 501–507.

Warren, S. G., 1982: Optical properties of snow. *Rev. Geophys. Space Phys.*, **20**, 67–89.

——, and W. J. Wiscombe, 1980: A model for the spectral albedo of snow. II: Snow containing atmospheric aerosols. *J. Atmos. Sci.*, **37**, 2734–2745.

WCRP, 1984a: *Scientific Plan for the World Climate Research Programme*, WCRP Publ. Ser. 2, WMO/TD-No. 6, World Meteorological Organization, 95 pp.

——, 1984b: *Development of the Implementation Plan for the International Satellite Land-Surface Climatology Project (ISLSCP) Phase I.* H-J. Bolle and S. I. Rasool, Eds., WMO/TD 46, World Meteorological Organization, 89 pp.

——, 1985: *Scientific Plan for the Tropical Ocean and Global Atmosphere Programme.* WMO/TD 64, WCRP Publ. Ser. 3, World Meteorological Organization, 147 pp.

Wetzel, P. J., D. Atlas and R. H. Woodward, 1984: Determining soil moisture from geosynchronous satellite infrared data: A feasibility study. *J. Climate Appl. Meteor.*, **23**, 375–391.

Wiscombe, W. J., and S. G. Warren, 1980: A model for the spectral albedo of snow. I: Pure snow. *J. Atmos. Sci.*, **37**, 2712–2733.

Wright, P., 1986: Problems in the use of ship observations for the study of interdecadal climate changes. *Mon. Wea. Rev.*, **114**, 1028–1034.

Yamanouchi, T., 1983: Variations of incident solar flux and snow albedo on the solar zenith angle and cloud cover, at Mizuho Station, Antarctica. *J. Meteor. Soc. Japan*, **61**, 879–893.

Zwally, H. J., J. C. Comiso, C. L. Parkinson, W. J. Campbell, F. D. Corsey and P. Gloersen, 1983: *Antarctic Sea Ice, 1973–1976: Satellite Passive-Microwave Observations.* NASA SP-459, National Aeronautical and Space Administration, Washington, DC, 206 pp.